

Article

Continuous Rotor Dynamics of Multi-Disc and Multi-Span Rotors: A Theoretical and Numerical Investigation of the Identification of Rotor Unbalance from Unbalance Responses

Aiming Wang ^{1,*}, Yujie Bi ², Yu Feng ¹, Jie Yang ¹, Xiaohan Cheng ¹ and Guoying Meng ¹

¹ School of Mechanical Electronic & Information Engineering, China University of Mining & Technology, Beijing 100083, China; fengyu20062009@163.com (Y.F.); 201702@cumtb.edu.cn (J.Y.); chengxh@cumtb.edu.cn (X.C.); mgy@cumtb.edu.cn (G.M.)

² School of Mechanics and Civil Engineering, China University of Mining & Technology, Beijing 100083, China; byjpengqiao@126.com

* Correspondence: wam_master@163.com; Tel.: +86-134-887-13431

Abstract: Rotor unbalance identification plays a critical role in balancing rotors. In this paper, concerned with multi-disc and multi-span rotor-bearing systems, two novel algorithms called the Single Direction Algorithm (SDA) and the Two Orthogonal Direction Algorithm (TODA) are proposed for identifying rotor unbalance from unbalance responses. A matrix method is proposed to solve the problem of the equations being non-linear transcendental, there being too many unknown variables in the equations, and rotor unbalances and bearing coefficients being coupled together. The unbalance responses at all the eccentric discs are necessary for identifying their unbalances. Numerical simulations are conducted to validate the proposed methods. Moreover, an adjustment point is found, and a proper sensor resolution is suggested to achieve high identification accuracy by means of numerical studies. In addition, the identification accuracy of SDA is better than TODA, and SDA is more practical and suitable for medium-speed and high-speed rotors. The proposed algorithms have the flexibility to incorporate any number of bearings and discs and provide a technique for monitoring rotor unbalance without test runs or external exciters.

Keywords: rotor unbalance; identification; multi-disc; multi-span; rotor-bearing systems



Citation: Wang, A.; Bi, Y.; Feng, Y.; Yang, J.; Cheng, X.; Meng, G. Continuous Rotor Dynamics of Multi-Disc and Multi-Span Rotors: A Theoretical and Numerical Investigation of the Identification of Rotor Unbalance from Unbalance Responses. *Appl. Sci.* **2022**, *12*, 3865. <https://doi.org/10.3390/app12083865>

Academic Editor: Jan Awrejcewicz

Received: 17 March 2022

Accepted: 8 April 2022

Published: 11 April 2022

Publisher's Note: MDPI stays neutral with regard to jurisdictional claims in published maps and institutional affiliations.



Copyright: © 2022 by the authors. Licensee MDPI, Basel, Switzerland. This article is an open access article distributed under the terms and conditions of the Creative Commons Attribution (CC BY) license (<https://creativecommons.org/licenses/by/4.0/>).

1. Introduction

1.1. Background and Formulation of the Problem

Rotating machines, such as steam turbine generators, turbine compressor units, pumps, etc., play a critical role in industry and are widely used. The rotor-bearing system (rotor) is the main element in rotating machines. Rotor unbalance is a typical fault of rotors. It is inevitable due to errors in manufacturing, installation, and operation. Vibrations and even sudden breakdowns can be caused because of rotor unbalance. Identifying rotor unbalance (amplitude and phase angle) is necessary for balancing rotors to reduce vibrations and ensure the safety of rotating machines. In view of these issues, rotor unbalance estimation, which is one inverse problem of rotor dynamics, has been an active area of research.

Although rotor unbalance can be estimated so that a rotor can be balanced off-site using a dynamic balancing machine in the laboratory, complex processes, such as uncovering, dismantling, and transporting, are required. The whole process is time-consuming and expensive and is difficult to implement, especially for large rotors. Hence, monitoring rotor unbalance on-line, by which means balancing time and cost can be reduced, is very important.

1.2. Literature Survey

Rotor unbalance identification is an old problem. The modal method proposed in 1959 [1,2] and the influence coefficient method proposed in 1964 [3] are the two classical

techniques used to solve the problem. Although they have been developed by many other researchers [4–13], test runs are still demanding. For large field rotors, starting and stopping the machine several times is costly and can reduce its service life [14].

Identifying rotor unbalance without test runs is the current trend [15]. This approach can be divided into two types: a method with external excitation and a method without external excitation. For the external excitation method, Bently and Muszynska [16] used frequency excitation to estimate rotor unbalance as well as bearing coefficients. Hiroshi Iida [17] applied impulse excitation on a double-disc and single-span rotor-bearing system to identify rotor unbalance as well as the stiffness and damping coefficients of two bearings. Lou [18,19] estimated rotor unbalance and bearing coefficients using an active magnetic exciter to generate external excitation. However, high-power exciters are necessary for large rotors and the excitation may damage the rotors.

Consequently, methods that do not require external excitation have been developed. Aiming at a single-span rotor-bearing system, Shrivastava and Mohanty [20] identified single-disc unbalance parameters from unbalance responses using an unbalance force estimation technique. A rotor unbalance estimation method using the joint-input state estimation technique [21] and least-squares technique was proposed [22] to solve the problem that the required response measurements at different locations on the shaft may not always be accessible. Yao [23] identified single-disc and double-disc unbalance based on modal expansion combined with optimisation algorithms. The errors caused by modal expansion were reduced by an integrated modal expansion inverse problem methodology combined with an optimisation procedure. Zou [24] developed a double-disc unbalance identification method using the finite element model combined with augmented Kalman filter algorithms. While based on the continuous dynamic model and analytical solution methods [25,26], Wang [27] provided an analytical model-based algorithm to identify single-disc unbalance. Moreover, some scholars have even tried to estimate rotor unbalance and bearing coefficients simultaneously without external excitation. Tiwari [28,29] formulated an estimation algorithm using unbalance responses from three different unbalance configurations for both clockwise and anti-clockwise rotor rotations. Wang [30] proposed a simultaneous estimation of the rotor unbalance and bearing coefficients of a continuous single-disc and single-span rotor-bearing system using the Rayleigh beam model. Jamadar [31] developed a mathematical model of an unbalanced rotor using dimensional analysis and a rigid rotor approach. The factorial regression analysis method is used to solve the model. Based on it, a numerical technique for the detection of unbalance magnitude has been proposed. Ambur [32] presented an estimation method for unbalance magnitude and phase from the vibration in frequency domain. Sanches [33] proposed an identification method of unbalance for a rotor with residual shaft bent based on the finite element method and correlation analysis. Zhang [34] proposed an unbalance identification method for a high-speed rotor without trial weights based on modal analysis and the modal equivalent principle. The shortcomings of the above-mentioned methods are that they cannot incorporate any number of bearings and discs.

Therefore, Bin [14] proposed an approach based on the multi-plane influence coefficient balancing method for multi-disc and multi-span rotors. Tiwari [35,36] developed an algorithm to simultaneously estimate the rotor unbalances, four stiffness coefficients, and four damping coefficients of bearings from impulse responses and run-down responses. However, test runs or external exciters are required in these studies.

1.3. Scope and Contribution of This Study

Focusing on multi-span and multi-disc rotors, two novel algorithms, called SDA and TODA, are proposed based on the continuous rotor dynamic analysis method (CRDAM) in this paper to realize rotor unbalance identification without excitation or test runs. These algorithms have the flexibility to incorporate any number of bearings and discs. The equations of the inverse problem, which are developed based on CRDAM using unbalance responses as inputs, cannot be directly solved to obtain rotor unbalances as the equations

are non-linear transcendental and there are too many unknown variables. Moreover, rotor unbalances and bearing coefficients are coupled together. A matrix method is proposed to solve the problem and identify rotor unbalance from unbalance responses. Four kinds of numerical simulations considering sensor resolutions and measurement errors are conducted for the validation. The adjustment point, which can greatly improve identification accuracy, is found by means of simulations. Proper sensor resolutions are recommended for engineering applications.

Compared with the methods described in references [14,35,36], SDA and TODA do not require test runs or external exciters. Compared with other existing methods in the literature, SDA and TODA can be applied to rotors with any number of bearings and any number of discs. Moreover, SDA and TODA can not only be used for rotors with rolling bearings but also for rotors supported by oil journal bearings. The proposed methods provide a technique for on-line monitoring of the rotor unbalances of multi-bearing and multi-disc rotors without using test runs or external exciters.

1.4. Organization of the Paper

Section 1 describes the background, the formulation of the problem, the literature, and the scope and contribution of this study. Section 2 discusses the derivation process of the proposed algorithms. Section 3 describes the numerical investigations for examining the algorithms and presents the discussion of the simulation results. Section 4 summarizes the conclusions of the study.

2. Theory

2.1. Revisiting the CRDAM

There are m discs and n bearings in the rotor shown in Figure 1. The unbalance response of any position on the rotor shaft can be expressed as a function of position, rotor unbalance, and bearing stiffness and damping coefficients, according to the CRDAM. Equations (1) and (2) represent the dimensionless form of the unbalance response in the frequency domain.

$$U(q) = \left\{ \sum_{j=1}^m \left[\pi \cdot m_{ju} \cdot \omega^2 \cdot e_j \cdot (\sin \alpha_j - j \cdot \cos \alpha_j) + \omega^2 \cdot m_{jd} L \cdot U_{jd} \right] \cdot G_u(q, q_{jd}) - \sum_{jj=1}^n L \left(k_{jj,yx} \cdot V_{jjb} + k_{jj,yy} \cdot U_{jjb} + i \cdot \omega \cdot c_{jj,yx} \cdot V_{jjb} + i \cdot \omega \cdot c_{jj,yy} \cdot U_{jjb} \right) G_u(q, q_{jjb}) \right\} \frac{L^2}{EI} \tag{1}$$

$$V(q) = \left\{ \sum_{j=1}^m \left[\pi \cdot m_{ju} \cdot \omega^2 \cdot e_j \cdot (\cos \alpha_j + i \cdot \sin \alpha_j) + \omega^2 \cdot m_{jd} L \cdot V_{jd} \right] G_v(q, q_{jd}) - \sum_{jj=1}^n L \left(k_{jj,xx} \cdot V_{jjb} + k_{jj,xy} \cdot U_{jjb} + i \cdot \omega \cdot c_{jj,xx} \cdot V_{jjb} + i \cdot \omega \cdot c_{jj,xy} \cdot U_{jjb} \right) G_v(q, q_{jjb}) \right\} \frac{L^2}{EI} \tag{2}$$

where $U(q)$ and $V(q)$ are the dimensionless unbalance response in the frequency domain along the y -axis and x -axis, respectively; m_{ju} are the eccentric masses of # j disc; e_j is the eccentric distance of # j disc; α_j are the eccentric angles, which are defined as the angles between the x -axis and the eccentric position in the direction of rotation; m_{jd} are the masses of # j disc; ω is the rotation frequency; L is the length of the shaft; E is the elastic modulus of the shaft; I is the diametric shaft cross-sectional geometric moment of inertia; $k_{jj,xx}$, $k_{jj,xy}$, $k_{jj,yx}$, and $k_{jj,yy}$ are the stiffness coefficients of # jj bearings respectively; $c_{jj,xx}$, $c_{jj,xy}$, $c_{jj,yx}$, and $c_{jj,yy}$ are the damping coefficients of # jj bearing, respectively; z is the axial position of the shaft; z_{jd} are the z coordinate positions of each disc; z_{jjb} is the z coordinate position of each bearing; q , q_{jd} , and q_{jjb} are their dimensionless values; $q = z/L$, $q_{jd} = z_{jd}/L$, $q_{jjb} = z_{jjb}/L$; $G_u(q, q_{jd})$, $G_u(q, q_{jjb})$, $G_v(q, q_{jd})$, and $G_v(q, q_{jjb})$ are Green's coefficients, which can be calculated using Green's functions $G_u(q, q_i)$ and $G_v(q, q_i)$; and Green's functions $G_u(q, q_i)$ and $G_v(q, q_i)$ can be found in reference [30]. Further, U_{jd} represents the dimensionless unbalance response of each disc in the frequency domain in the y direction; V_{jd} represents the dimensionless unbalance response of each disc in the

frequency domain in the x direction; U_{jyb} represents the dimensionless unbalance response of each bearing in the frequency domain in the y direction; V_{jyb} represents the dimensionless unbalance response of each bearing in the frequency domain in the x direction.

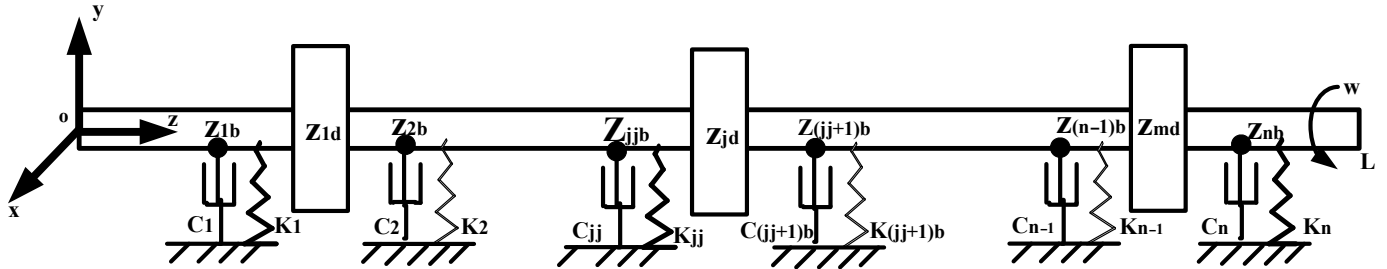


Figure 1. A multi-disc and multi-span rotor-bearing system.

2.2. Single Direction Algorithm

Identification of rotor unbalance amplitude $m_{ju} \cdot e_j$ and angle α_j is the inverse problem of the CRDAM. According to Equations (1) and (2), the relationships between unbalance response and rotor unbalance and the bearing coefficients are non-linear transcendental, although the eight stiffness and damping coefficients of the bearing are linearized. As the number of bearings and discs are unknown, the numbers of equations and unknown variables are also unknown. Moreover, rotor unbalance and bearing coefficients are coupled together according to Equations (1) and (2). Although enough equations can be obtained by using the unbalance responses as inputs and considering rotor unbalances and bearings coefficients as unknown variables, they cannot be solved directly to obtain the unknown variables (amplitude and angle of rotor unbalance) due to the non-linear transcendental equations, the unfixed number of equations, and the unknown variables. Hence, it is proposed that Equation (1) is written in matrix form as follows:

$$\frac{U(q) \cdot EI}{L^2} = \begin{bmatrix} G_u(q, q_{1d}) \\ \vdots \\ G_u(q, q_{md}) \\ G_u(q, q_{1b}) \\ \vdots \\ G_u(q, q_{nb}) \end{bmatrix}^T \cdot \begin{bmatrix} \pi \cdot \omega^2 \cdot m_{1u} e_1 \cdot (\sin \alpha_1 - i \cdot \cos \alpha_1) + L \cdot \omega^2 \cdot m_{1d} U_{1d} \\ \vdots \\ \pi \cdot \omega^2 \cdot m_{mu} e_m \cdot (\sin \alpha_m - i \cdot \cos \alpha_m) + L \cdot \omega^2 \cdot m_{md} U_{md} \\ -L \cdot k_{1s-yx} \cdot V_{1b} - L \cdot k_{1s-yy} \cdot U_{1b} \\ \vdots \\ -L \cdot k_{ns-yx} \cdot V_{nb} - L \cdot k_{ns-yy} \cdot U_{nb} \end{bmatrix}_{m+n} \quad (3)$$

$m + n$ equations can be obtained based on Equation (3) by using $m + n$ unbalance responses as inputs. There are two unknown variables (amplitude and angle) for a disc's unbalance. Moreover, the eight coefficients of a bearing are also unknown. Hence, there are $2 \cdot m + 8 \cdot n$ unknown variables for a rotor with m discs and n bearings, while only $m + n$ equations exist. The greatest difficulty is due to the fact that the relationship among these variables is non-linear transcendental. A direct solution is not feasible. Therefore, by writing the $m + n$ equations in matrix form, Equation (4) can be obtained as the following:

$$\frac{EI}{L^2} \begin{bmatrix} U(q_{1s}) \\ \vdots \\ U(q_{ms}) \\ U(q_{(m+1)s}) \\ \vdots \\ U(q_{(m+n)s}) \end{bmatrix} = H_1 \cdot \begin{bmatrix} \pi \cdot \omega^2 \cdot m_{1u} e_1 \cdot (\sin \alpha_1 - i \cdot \cos \alpha_1) + L \cdot \omega^2 \cdot m_{1d} U_{1d} \\ \vdots \\ \pi \cdot \omega^2 \cdot m_{mu} e_m \cdot (\sin \alpha_m - i \cdot \cos \alpha_m) + L \cdot \omega^2 \cdot m_{md} U_{md} \\ -L \cdot k_{1s-yx} \cdot V_{1b} - L \cdot k_{1s-yy} \cdot U_{1b} \\ \vdots \\ -L \cdot k_{ns-yx} \cdot V_{nb} - L \cdot k_{ns-yy} \cdot U_{nb} \end{bmatrix}_{m+n} \quad (4)$$

where q_{1s}, \dots, q_{ms} and $q_{(m+1)s}, \dots, q_{(m+n)s}$ are the dimensionless values of locations on the shaft excluding the locations of all discs and bearings; $U(q_{1s}), \dots, U(q_{ms})$ and $U(q_{(m+1)s}), \dots, U(q_{(m+n)s})$ are the measured dimensionless unbalance responses in the frequency domain in the y direction of locations, excluding all discs and bearings; the number of $U(q_{1s}), \dots, U(q_{ms})$ is m and the number of $U(q_{(m+1)s}), \dots, U(q_{(m+n)s})$ is n ; H_1 is a

$(m + n) \times (m + n)$ matrix and can be calculated using Green’s functions $G_u(q, q_i)$ as long as the locations of the measuring points, the bearings, and the discs are known; H_1 is as follows:

$$H_1 = \begin{bmatrix} G_u(q_{1s}, q_{1d}) & \cdots & G_u(q_{1s}, q_{md}) & G_u(q_{1s}, q_{1b}) & \cdots & G_u(q_{1s}, q_{nb}) \\ \vdots & \vdots & \vdots & \vdots & \vdots & \vdots \\ G_u(q_{ms}, q_{1d}) & \cdots & G_u(q_{ms}, q_{md}) & G_u(q_{ms}, q_{1b}) & \cdots & G_u(q_{ms}, q_{nb}) \\ G_u(q_{(m+1)s}, q_{1d}) & \cdots & G_u(q_{(m+1)s}, q_{md}) & G_u(q_{(m+1)s}, q_{1b}) & \cdots & G_u(q_{(m+1)s}, q_{nb}) \\ \vdots & \cdots & \vdots & \vdots & \cdots & \vdots \\ G_u(q_{(m+n)s}, q_{1d}) & \cdots & G_u(q_{(m+n)s}, q_{md}) & G_u(q_{(m+n)s}, q_{1b}) & \cdots & G_u(q_{(m+n)s}, q_{nb}) \end{bmatrix}_{(m+n) \times (m+n)}$$

Equation (5) can be obtained according to Equation (4).

$$\begin{bmatrix} \pi \cdot \omega^2 \cdot m_{1u} e_1 \cdot (\sin \alpha_1 - i \cdot \cos \alpha_1) + L \cdot \omega^2 \cdot m_{1d} U_{1d} \\ \vdots \\ \pi \cdot \omega^2 \cdot m_{mu} e_m \cdot (\sin \alpha_m - i \cdot \cos \alpha_m) + L \cdot \omega^2 \cdot m_{md} U_{md} \\ -L \cdot k_{1s \cdot yx} \cdot V_{1b} - L \cdot k_{1s \cdot yy} \cdot U_{1b} \\ \vdots \\ -L \cdot k_{ns \cdot yx} \cdot V_{nb} - L \cdot k_{ns \cdot yy} \cdot U_{nb} \end{bmatrix}_{m+n} = \frac{EI}{L^2} \cdot H_1^{-1} \begin{bmatrix} U(q_{1s}) \\ \vdots \\ U(q_{ms}) \\ U(q_{(m+1)s}) \\ \vdots \\ U(q_{(m+n)s}) \end{bmatrix} \tag{5}$$

The right side of Equation (5) is known. Define H_2 as following.

$$H_2 = \frac{EI}{L^2} \cdot H_1^{-1} \begin{bmatrix} U(q_{1s}) \\ \vdots \\ U(q_{ms}) \\ U(q_{(m+1)s}) \\ \vdots \\ U(q_{(m+n)s}) \end{bmatrix}$$

Equation (6) is obtained according to Equation (5).

$$\begin{cases} \pi \cdot \omega^2 \cdot m_{1u} e_1 \cdot (\sin \alpha_1 - i \cdot \cos \alpha_1) + L \cdot \omega^2 \cdot m_{1d} U_{1d} = H_2(1, 1) \\ \vdots \\ \pi \cdot \omega^2 \cdot m_{mu} e_m \cdot (\sin \alpha_m - i \cdot \cos \alpha_m) + L \cdot \omega^2 \cdot m_{md} U_{md} = H_2(m, 1) \end{cases} \tag{6}$$

According to Equations (6) and (7) is obtained.

$$\begin{cases} m_{1u} e_1 \cdot (\sin \alpha_1 - i \cdot \cos \alpha_1) = \frac{[H_2(1,1) - L \cdot \omega^2 \cdot m_{1d} U_{1d}]}{\pi \cdot \omega^2} \\ \vdots \\ m_{mu} e_m \cdot (\sin \alpha_m - i \cdot \cos \alpha_m) = \frac{[H_2(m,1) - L \cdot \omega^2 \cdot m_{md} U_{md}]}{\pi \cdot \omega^2} \end{cases} \tag{7}$$

According to Equations (7)–(9) are obtained.

$$\begin{cases} m_{1u} e_1 = \left| \frac{[H_2(1,1) - L \cdot \omega^2 \cdot m_{1d} U_{1d}]}{\pi \cdot \omega^2} \right| \\ \vdots \\ m_{mu} e_m = \left| \frac{[H_2(m,1) - L \cdot \omega^2 \cdot m_{md} U_{md}]}{\pi \cdot \omega^2} \right| \end{cases} \tag{8}$$

$$\begin{cases} \sin \alpha_1 - i \cdot \cos \alpha_1 = \frac{[H_2(1,1) - L \cdot \omega^2 \cdot m_{1d} U_{1d}]}{[H_2(1,1) - L \cdot \omega^2 \cdot m_{1d} U_{1d}]} \\ \vdots \\ \sin \alpha_m - i \cdot \cos \alpha_m = \frac{[H_2(m,1) - L \cdot \omega^2 \cdot m_{md} U_{md}]}{[H_2(m,1) - L \cdot \omega^2 \cdot m_{md} U_{md}]} \end{cases} \quad (9)$$

Equation (8) is the amplitude of rotor unbalance for each eccentric disc. Moreover, according to Equations (9) and (10) can be obtained, by means of which the angle of rotor unbalance for each eccentric disc can be calculated.

$$\begin{cases} \alpha_1 = \text{angle} \left(-\text{imag} \left(\frac{[H_2(1,1) - L \cdot \omega^2 \cdot m_{1d} U_{1d}]}{\pi \cdot \omega^2} \right) + i \cdot \text{real} \left(\frac{[H_2(1,1) - L \cdot \omega^2 \cdot m_{1d} U_{1d}]}{\pi \cdot \omega^2} \right) \right) \\ \vdots \\ \alpha_m = \text{angle} \left(-\text{imag} \left(\frac{[H_2(m,1) - L \cdot \omega^2 \cdot m_{md} U_{md}]}{\pi \cdot \omega^2} \right) + i \cdot \text{real} \left(\frac{[H_2(m,1) - L \cdot \omega^2 \cdot m_{md} U_{md}]}{\pi \cdot \omega^2} \right) \right) \end{cases} \quad (10)$$

where angle () is the function used to obtain the angle of a complex number, real () is the real part of a complex number, and imag () is the imaginary part of a complex number.

Hence, the amplitude and angle of each eccentric disc’s unbalance can be calculated based on Equations (8) and (10), in which the unbalance responses in the *y* direction are required as inputs. According to Equations (4) and (5), the matrix *H*₂ in Equations (8) and (10) can be calculated using *m* + *n* unbalance responses as inputs. The unbalance response of the eccentric disc whose unbalance is to be identified must be measured according to Equation (7). Hence, the total number of input unbalance responses is equal to *m* + *n* + 1. To identify all the eccentric discs’ unbalances simultaneously, the unbalance responses of all the discs should be included.

Similarly, Equation (11) can be obtained according to Equation (2) in the *x* direction.

$$\frac{V(q) \cdot EI}{L^2} = \begin{bmatrix} G_v(q, q_{1d}) \\ \vdots \\ G_v(q, q_{md}) \\ G_v(q, q_{1b}) \\ \vdots \\ G_v(q, q_{(m+n)b}) \end{bmatrix}^T \begin{bmatrix} \pi \cdot \omega^2 \cdot m_{u1} \cdot e_1 \cdot (\cos \alpha_1 + i \cdot \sin \alpha_1) + \omega^2 \cdot m_{1d} L \cdot V_{1d} \\ \vdots \\ \pi \cdot \omega^2 \cdot m_{mu} \cdot e_m \cdot (\cos \alpha_m + i \cdot \sin \alpha_m) + \omega^2 \cdot m_{md} L \cdot V_{md} \\ -L \cdot k_{1s \cdot xy} U_{1b} - L \cdot k_{1s \cdot xx} V_{1b} \\ \vdots \\ -L \cdot k_{ns \cdot xy} U_{nb} - L \cdot k_{ns \cdot xx} V_{nb} \end{bmatrix}_{m+n} \quad (11)$$

m + *n* equations can be obtained based on Equation (11) using the unbalance responses as inputs and considering rotor unbalances and bearing coefficients as unknown variables. Equation (12) can be obtained by writing the equations in matrix form.

$$\frac{EI}{L^2} \cdot \begin{bmatrix} V(q_{1s}) \\ \vdots \\ V(q_{ms}) \\ V(q_{(m+1)s}) \\ \vdots \\ V(q_{ns}) \end{bmatrix} = H_3 \cdot \begin{bmatrix} \pi \cdot \omega^2 \cdot m_{u1} \cdot e_1 \cdot (\cos \alpha_1 + i \cdot \sin \alpha_1) + \omega^2 \cdot m_{1d} L \cdot V_{1d} \\ \vdots \\ \pi \cdot \omega^2 \cdot m_{mu} \cdot e_m \cdot (\cos \alpha_m + i \cdot \sin \alpha_m) + \omega^2 \cdot m_{md} L \cdot V_{md} \\ -L \cdot k_{1s \cdot xy} U_{1b} - L \cdot k_{1s \cdot xx} V_{1b} \\ \vdots \\ -L \cdot k_{ns \cdot xy} U_{nb} - L \cdot k_{ns \cdot xx} V_{nb} \end{bmatrix}_{m+n} \quad (12)$$

where *V*(*q*_{1*s*}), . . . , *V*(*q*_{*m**s*}) and *V*(*q*_{(*m*+1)*s*}), . . . , *V*(*q*_{(*m*+*n*)*s*}) are the measured dimensionless unbalance responses in the frequency domain in the *y* direction of locations, excluding the discs and bearings; the number of *V*(*q*_{1*s*}), . . . , *V*(*q*_{*m**s*}) is *m* and the number of *V*(*q*_{(*m*+1)*s*}), . . . , *V*(*q*_{*n**s*}) is *n*; *H*₃ is a (*m* + *n*) × (*m* + *n*) matrix and can be calculated using Green’s functions *G*_{*v*}(*q*, *q*_{*i*}) as long as the locations of the measuring points, the bearings, and the discs are known; *H*₃ is as follows:

$$H_3 = \begin{bmatrix} G_v(q_{1s}, q_{1d}) & \cdots & G_v(q_{1s}, q_{md}) & G_v(q_{1s}, q_{1b}) & \cdots & G_v(q_{1s}, q_{nb}) \\ G_v(q_{ms}, q_{1d}) & & G_v(q_{ms}, q_{md}) & G_v(q_{ms}, q_{1b}) & & G_v(q_{ms}, q_{nb}) \\ G_v(q_{(m+1)s}, q_{1d}) & & G_v(q_{(m+1)s}, q_{md}) & G_v(q_{(m+1)s}, q_{1b}) & & G_v(q_{(m+1)s}, q_{nb}) \\ G_v(q_{ns}, q_{1d}) & & G_v(q_{ns}, q_{md}) & G_v(q_{ns}, q_{1b}) & & G_v(q_{ns}, q_{nb}) \end{bmatrix}.$$

Hence, Equation (13) is obtained.

$$\begin{bmatrix} \pi \cdot \omega^2 \cdot m_{u1} \cdot e_1 \cdot (\cos \alpha_1 + i \cdot \sin \alpha_1) + \omega^2 \cdot m_{1d}L \cdot V_{1d} \\ \vdots \\ \pi \cdot \omega^2 \cdot m_{mu} \cdot e_m \cdot (\cos \alpha_m + i \cdot \sin \alpha_m) + \omega^2 \cdot m_{md}L \cdot V_{md} \\ -L \cdot k_{1s.xy}U_{1b} - L \cdot k_{1s.xx}V_{1b} \\ \vdots \\ -L \cdot k_{ns.xy}U_{nb} - L \cdot k_{ns.xx}V_{nb} \end{bmatrix}_{m+n} = \frac{EI}{L^2} \cdot H_3^{-1} \begin{bmatrix} V(q_{1s}) \\ \vdots \\ V(q_{(m+1)s}) \\ \vdots \\ V(q_{ns}) \end{bmatrix} \tag{13}$$

Define H_4 as following.

$$H_4 = \frac{EI}{L^2} \cdot H_3^{-1} \begin{bmatrix} V(q_{1s}) \\ \vdots \\ V(q_{(m+1)s}) \\ \vdots \\ V(q_{ns}) \end{bmatrix}.$$

According to Equations (13) and (14) can be obtained.

$$\begin{cases} \pi \cdot \omega^2 \cdot m_{u1} \cdot e_1 \cdot (\cos \alpha_1 + i \cdot \sin \alpha_1) + \omega^2 \cdot m_{1d}L \cdot V_{1d} = H_4(1, 1) \\ \vdots \\ \pi \cdot \omega^2 \cdot m_{mu} \cdot e_m \cdot (\cos \alpha_m + i \cdot \sin \alpha_m) + \omega^2 \cdot m_{md}L \cdot V_{md} = H_4(m, 1) \end{cases} \tag{14}$$

According to Equations (14) and (15) can be obtained.

$$\begin{cases} m_{u1} \cdot e_1 \cdot (\cos \alpha_1 + i \cdot \sin \alpha_1) = \frac{[H_4(1,1) - \omega^2 \cdot m_{1d}L \cdot V_{1d}]}{\pi \cdot \omega^2} \\ \vdots \\ m_{mu} \cdot e_m \cdot (\cos \alpha_m + i \cdot \sin \alpha_m) = \frac{[H_4(m,1) - \omega^2 \cdot m_{md}L \cdot V_{md}]}{\pi \cdot \omega^2} \end{cases} \tag{15}$$

According to Equations (15)–(17) are obtained, by means of which the amplitude and angle of the rotor unbalance can be calculated. The unbalance responses in the x direction are used as inputs. To calculate the matrix H_4 , the number of measured unbalance responses should be $m + n$ according to Equations (12) and (13). To identify an eccentric disc’s unbalance, its unbalance response should also be measured. Therefore, the total amount of the measured unbalance responses is $m + n + 1$ and the unbalance responses of all the discs should be measured in order to estimate all the eccentric discs’ unbalances.

$$\begin{cases} m_{u1} \cdot e_1 = \left| \frac{[H_4(1,1) - \omega^2 \cdot m_{1d}L \cdot V_{1d}]}{\pi \cdot \omega^2} \right| \\ \vdots \\ m_{mu} \cdot e_m = \left| \frac{[H_4(m,1) - \omega^2 \cdot m_{md}L \cdot V_{md}]}{\pi \cdot \omega^2} \right| \end{cases} \tag{16}$$

$$\begin{cases} \alpha_1 = \text{angle}\left(\frac{[H_4(1,1) - \omega^2 \cdot m_{1d} L \cdot V_{1d}]}{\pi \cdot \omega^2}\right) \\ \vdots \\ \alpha_m = \text{angle}\left(\frac{[H_4(m,1) - \omega^2 \cdot m_{md} L \cdot V_{md}]}{\pi \cdot \omega^2}\right) \end{cases} \tag{17}$$

2.3. Two Orthogonal Direction Algorithms

According to Equations (6) and (14), Equation (18) can be obtained.

$$\begin{cases} \frac{H_2(1,1) - \pi \cdot \omega^2 \cdot m_{1u} e_1 \cdot (\sin \alpha_1 - i \cdot \cos \alpha_1)}{H_4(1,1) - \pi \cdot \omega^2 \cdot m_{u1} \cdot e_1 \cdot (\cos \alpha_1 + i \cdot \sin \alpha_1)} = \frac{U_{1d}}{V_{1d}} = C_{1d} \\ \vdots \\ \frac{H_2(m,1) - \pi \cdot \omega^2 \cdot m_{mu} e_m \cdot (\sin \alpha_m - i \cdot \cos \alpha_m)}{H_4(m,1) - \pi \cdot \omega^2 \cdot m_{mu} \cdot e_m \cdot (\cos \alpha_m + i \cdot \sin \alpha_m)} = \frac{U_{md}}{V_{md}} = C_{md} \end{cases} \tag{18}$$

Let $\begin{cases} cx_1 = m_{1u} e_1 \cdot \sin \alpha_1 \\ cy_1 = m_{1u} e_1 \cdot \cos \alpha_1 \end{cases}$ \vdots . According to Equations (18) and (19) is obtained.

$$\begin{cases} \begin{cases} cx_m = m_{mu} e_m \cdot \sin \alpha_m \\ cy_m = m_{mu} e_m \cdot \cos \alpha_m \end{cases} \\ \begin{cases} H_2(1,1) - \pi \cdot \omega^2 \cdot (cx_1 - i \cdot cy_1) = C_{1d} \cdot H_4(1,1) - C_{1d} \cdot \pi \cdot \omega^2 \cdot m_{u1} \cdot e_1 \cdot (cy_1 + i \cdot cx_1) \\ \vdots \\ H_2(m,1) - \pi \cdot \omega^2 \cdot (cx_m - i \cdot cy_m) = C_{md} \cdot H_4(m,1) - C_{md} \cdot \pi \cdot \omega^2 \cdot (cy_m + i \cdot cx_m) \end{cases} \end{cases} \tag{19}$$

In Equation (19), $H_2(1,1) \cdots H_2(m,1), H_4(1,1) \cdots H_4(m,1), C_{1d} \cdots C_{md}$ are complex numbers and the others are real numbers. According to Equations (19) and (20) can be obtained.

$$\begin{cases} \pi \cdot \omega^2 \cdot \begin{bmatrix} -(1 + iC_{1d}) & rC_{1d} \\ rC_{1d} & (1 + iC_{1d}) \end{bmatrix} \cdot \begin{bmatrix} cx_1 \\ cy_1 \end{bmatrix} = \begin{bmatrix} r(C_{1d}H_4(1,1)) - rH_2(1,1) \\ i(C_{1d}H_4(1,1)) - iH_2(1,1) \end{bmatrix} \\ \vdots \\ \pi \cdot \omega^2 \cdot \begin{bmatrix} -(1 + iC_{md}) & rC_{md} \\ rC_{md} & (1 + iC_{md}) \end{bmatrix} \cdot \begin{bmatrix} cx_m \\ cy_m \end{bmatrix} = \begin{bmatrix} r(C_{md}H_4(m,1)) - rH_2(m,1) \\ i(C_{md}H_4(m,1)) - iH_2(m,1) \end{bmatrix} \end{cases} \tag{20}$$

where $rH_2(1,1) \cdots rH_2(m,1), rH_4(1,1) \cdots rH_4(m,1), rC_{1d} \cdots rC_{md}$ are the real parts of the above-mentioned complex number; and $iH_2(1,1) \cdots iH_2(m,1), iH_4(1,1) \cdots iH_4(m,1), iC_{1d} \cdots iC_{md}$ are the imaginary parts of the above-mentioned complex number.

Hence, Equation (21) is obtained according to Equation (20).

$$\begin{cases} \begin{bmatrix} cx_1 \\ cy_1 \end{bmatrix} = \frac{1}{\pi \cdot \omega^2} \cdot \begin{bmatrix} -(1 + iC_{1d}) & rC_{1d} \\ rC_{1d} & (1 + iC_{1d}) \end{bmatrix}^{-1} \begin{bmatrix} r(C_{1d}H_4(1,1)) - rH_2(1,1) \\ i(C_{1d}H_4(1,1)) - iH_2(1,1) \end{bmatrix} \\ \vdots \\ \begin{bmatrix} cx_m \\ cy_m \end{bmatrix} = \frac{1}{\pi \cdot \omega^2} \cdot \begin{bmatrix} -(1 + iC_{md}) & rC_{md} \\ rC_{md} & (1 + iC_{md}) \end{bmatrix}^{-1} \begin{bmatrix} r(C_{md}H_4(m,1)) - rH_2(m,1) \\ i(C_{md}H_4(m,1)) - iH_2(m,1) \end{bmatrix} \end{cases} \tag{21}$$

The amplitude and angle of the rotor unbalance are:

$$\begin{cases} \begin{cases} m_{1u} e_1 = \text{abs}(cy_1 + i \cdot cx_1) \\ \alpha_1 = \text{angle}(cy_1 + i \cdot cx_1) \end{cases} \\ \vdots \\ \begin{cases} m_{mu} e_m = \text{abs}(cy_m + i \cdot cx_m) \\ \alpha_m = \text{angle}(cy_m + i \cdot cx_m) \end{cases} \end{cases} \tag{22}$$

where $\text{abs}()$ is the function used to obtain the module of a complex number and $\text{angle}()$ is the function used to obtain the angle of a complex number.

Therefore, the amplitude and angle of each eccentric disc's unbalance can be calculated based on Equations (21) and (22). There should be $m + n$ unbalance responses in both the x and y directions to obtain the matrix H_2 and H_4 . If an eccentric disc's unbalance is to be identified, its unbalance responses in both the x and y directions are required according to Equation (18). Hence, there should be $m + n + 1$ measured unbalance responses in the two orthogonal directions. To identify all the eccentric discs' unbalances, the unbalance responses of the measured eccentric discs must be included.

2.4. Identification Procedures of the Two Algorithms

The identification procedures used in SDA and TODA to estimate the rotor unbalances ($m_{uj} \cdot e_j, \alpha_j$) of all discs are defined in Figure 2.

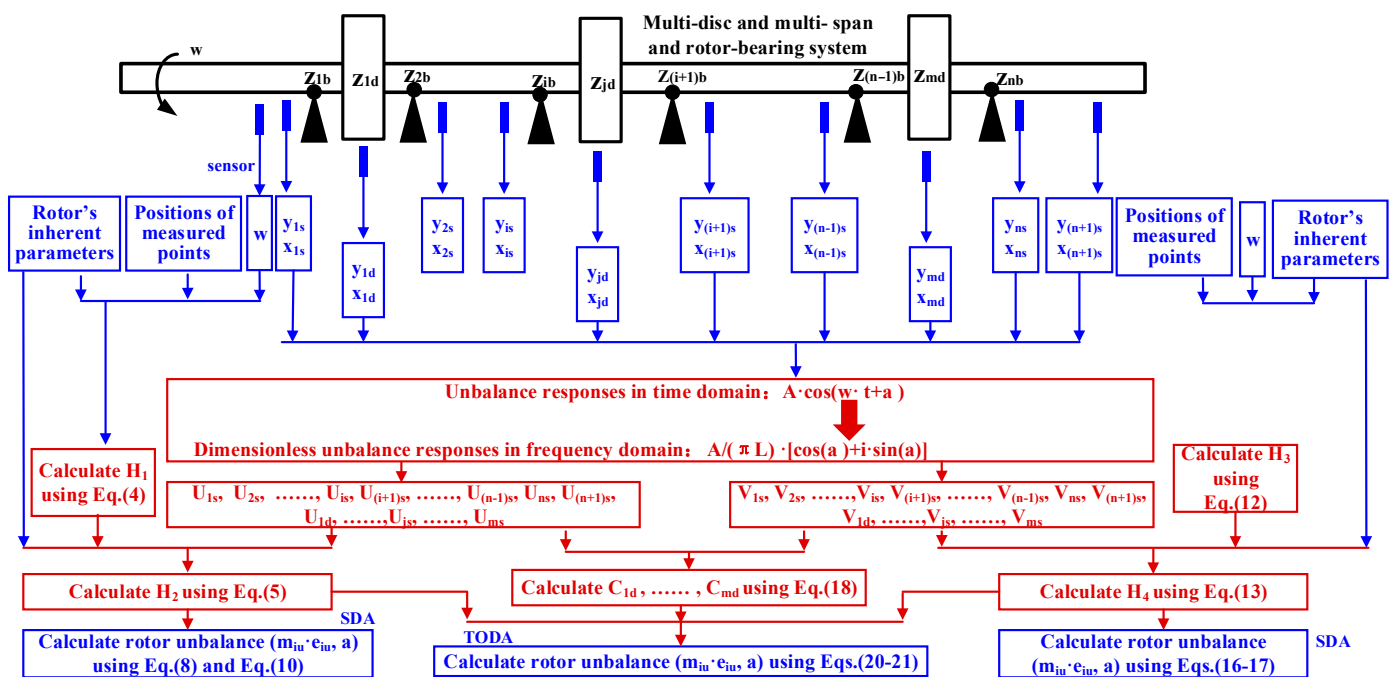


Figure 2. Identification procedures of SDA and TODA.

Firstly, each disc's unbalance response and the other $n + 1$ unbalance responses should be measured and changed to dimensionless unbalance responses in the frequency domain according to Equation (23). Meanwhile, the rotating speed should also be measured. The inherent parameters, which are the length of the shaft, the mass per unit length of the rotor shaft, the elastic modulus of the shaft, and the diameter of the shaft, should be known, as prior knowledge and the location of the selected measured points on the shaft should also be used as inputs.

Secondly, the matrix H_1 and H_3 could be calculated according to Equations (4) and (12), respectively. Then, H_2 and H_4 can be calculated according to Equations (5) and Equation (13), respectively.

Thirdly, using H_2 and the dimensionless unbalance responses in the y direction in frequency domain obtained in the first step, each disc's unbalance can be calculated according to Equations (8) and (10). Or, using H_4 and the dimensionless unbalance responses in the x direction in the frequency domain obtained in the first step, each disc's unbalance can be calculated according to Equations (16) and (17). This is the identification procedure used in SDA. While for TODA, C_{1d}, \dots, C_{md} should be calculated using the dimensionless unbalance responses in the frequency domain in both the x and y directions according to

Equation (18). Then, using H_2 and H_4 , all rotor unbalances can be calculated based on Equations (20) and (21).

$$UD = \frac{A}{\pi L} [\cos(\alpha) + i \cdot \sin(\alpha)] \tag{23}$$

where UD is the dimensionless unbalance response in the frequency domain; and A and α are the amplitude and phase of the unbalance responses in the time domain, respectively.

3. Numerical Simulations and Discussion

3.1. Methodology of the Numerical Simulations

The numerical simulations were conducted to validate the proposed methods by comparing the identified rotor unbalances with the set value of rotor unbalances.

As shown in Figures 3 and 4, six computational examples, which represent single-span and single-disc rotors (g1.1, h1.1), single-span and four-disc rotors (g1.4, h1.4), and four-span and four-disc rotors (g4.4, h4.4) are used in the simulation. The rotors g1.1, g1.4, and g4.4 are supported by rolling bearings, and h1.1, h1.4, and h4.4 are sustained by oil journal bearings. The parameters of the rotors are summarized in Tables 1–6. The positions of each bearing and disc on the shaft are shown in Figures 3 and 4. There are 121 nodes in the rotors in Figure 3 by dividing the shaft into 120 segments equally. There are 61 nodes in the rotors in Figure 4 by dividing the shaft into 60 segments equally. All the nodes, where the bearings and the discs located, are chosen for calculating simulated unbalance response by the CRDAM. Moreover, besides the above points, any other point on the shaft is also chosen in the simulation.

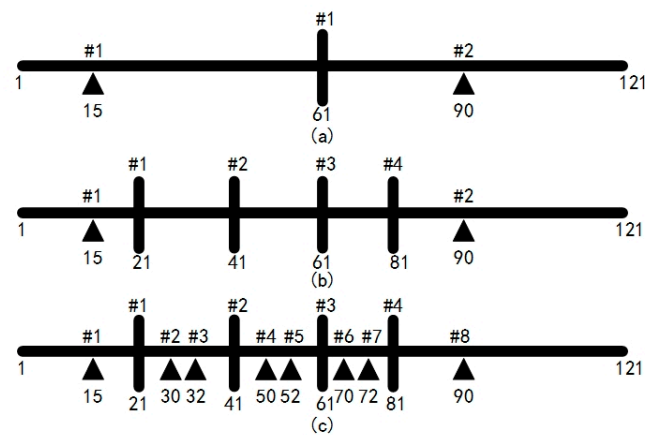


Figure 3. Rotors supported by rolling bearings: (a) single-span single-disc rotor (g1.1); (b) single-span four-disc rotor (g1.4); (c) four-span four-disc rotor (g4.4).

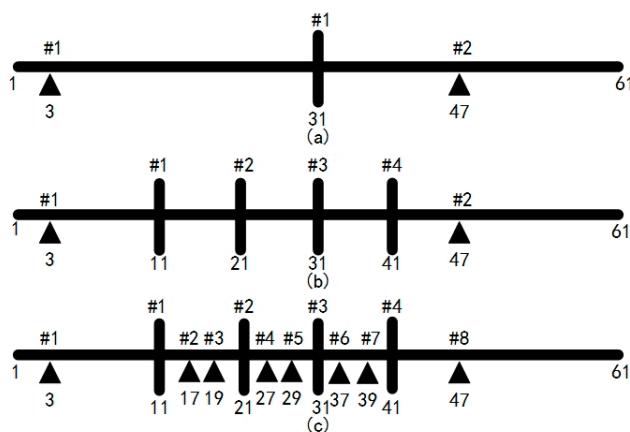


Figure 4. Rotors supported by oil journal bearings: (a) single-span single-disc rotor (h1.1); (b) single-span four-disc rotor (h1.4); (c) four-span four-disc rotor (h4.4).

Table 1. Meanings of symbols in the computational example of the rotor.

Parameter	Meaning
r_shaft	Radius of the shaft
p_shaft	Density of the shaft
E_shaft	Elastic modulus of the shaft
L_shaft	Length of the shaft
r_disc	Radius of the disc
p_disc	Density of the disc
E_disc	Elastic modulus of the disc
L_disc	Width of the disc

Table 2. Parameters of the rotor shafts in the rotors.

Parameter	Value	Parameter	Value
r_shaft of rotor g1.1, g1.4 and g4.4	10×10^{-3} m	L_shaft of the rotor g1.4	1200×10^{-3} m
r_shaft of rotor h1.1, h1.4 and h4.4	15×10^{-3} m	L_shaft of the rotor g4.4	1600×10^{-3} m
p_shaft	7800 kgm^{-3}	L_shaft of the rotor h1.1	1400×10^{-3} m
E_shaft	2.1×10^{11} Pa	L_shaft of the rotor h1.4	1400×10^{-3} m
L_shaft of the rotor g1.1	800×10^{-3} m	L_shaft of the rotor h4.4	3600×10^{-3} m

Table 3. Parameters of the eccentric discs in the rotors g1.1, g1.4, and g4.4.

Parameter	Value	Parameter	Value	Parameter	Value
m_{1u}	0.12031 kg	m_{2u}	0.15 kg	m_{3u}	0.01 kg
e_1	50×10^{-3} m	e_2	10×10^{-3} m	e_3	20×10^{-3} m
α_1	225°	α_2	120°	α_3	-120°
m_{4u}	0.10 kg	r_disc of #1 disc	60×10^{-3} m	p_disc of of #1~#4 disc	7800 kgm^{-3}
e_4	15×10^{-3} m	r_disc of #2~#4	50×10^{-3} m	E_disc of of #1~#4 disc	2.1×10^{11} Pa
α_4	-170°	L_disc of of #1~#4 disc	10×10^{-3} m		

Table 4. Parameters of the eccentric discs in the rotors h1.1, h1.4, and h4.4.

Parameter	Value	Parameter	Value	Parameter	Value
m_{1u}	0.05 kg	m_{2u}	0.15 kg	m_{3u}	0.01 kg
e_1	30×10^{-3} m	e_2	10×10^{-3} m	e_3	20×10^{-3} m
α_1	45°	α_2	90°	α_3	170°
m_{4u}	0.10 kg	r_disc of #1~4 disc	50×10^{-3} m	p_disc of of #1~#4 disc	7800 kgm^{-3}
e_4	15×10^{-3} m	L_disc of of #1~#4 disc	10×10^{-3} m		
α_4	-170°	E_disc of of #1~#4 disc	2.1×10^{11} Pa		

Four kinds of numerical simulations were conducted. Firstly, the simulated unbalance responses calculated by the CRDAM were directly fed into SDA and TODA to estimate rotor unbalances. Secondly, a similar identification exercise was performed by contaminating simulated unbalance responses by the set measured error. The relative error for the unbalance response amplitude was 5% and the absolute error for the unbalance response angle was 5° . Thirdly, the resolution of the vibration displacement sensor should be considered when measuring the unbalance response. Hence, identification exercises were performed by contaminating simulated unbalance responses at a resolution of 0.1 nm, which is the

highest used at present. Finally, identification exercises were performed considering four kinds of typical sensor resolution (0.1 nm, 1 nm, 0.1 μm, and 1 μm). By limiting the number of digits after the decimal point in the unbalance responses, the resolutions of unbalance response measurement systems are considered.

In the above simulations, the calculation frequency was from 1 to 2001 Hz and the interval was 2 Hz. The relative error for the identified rotor unbalance amplitude to the set rotor unbalance amplitude and the absolute error for the identified rotor unbalance angle to the set rotor unbalance angle were used for the analysis of the simulation results. Moreover, the statistical results of the allowable frequency points (AFPs), at which the identification error for the rotor unbalance amplitude was less than 20% and the rotor unbalance angle was less than 10°, were obtained.

In addition, as shown in Figure 2, SDA includes two algorithms which are represented by Equations (8), (10), (16), and (17), respectively. The difference between them is that one requires unbalance responses in the *y* direction as input and the other uses unbalance responses in the *x* direction. They can be considered the same algorithm. Hence, for SDA, only Equations (8) and (10), which require unbalance responses in the *y* direction, are validated by the simulations.

Table 5. Parameters of the eight oil journal bearings in the rotors.

Parameter	Value	Parameter	Value
$\begin{bmatrix} k_{1.xx} & k_{1.xy} \\ k_{1.yx} & k_{1.yy} \end{bmatrix}$	$\begin{bmatrix} 9 \times 10^6 & 1 \times 10^6 \\ -6 \times 10^6 & 4 \times 10^6 \end{bmatrix}$ N/m	$\begin{bmatrix} k_{2.xx} & k_{2.xy} \\ k_{2.yx} & k_{2.yy} \end{bmatrix}$	$\begin{bmatrix} 3 \times 10^6 & 0.6 \times 10^6 \\ -1.5 \times 10^6 & 1 \times 10^6 \end{bmatrix}$ N/m
$\begin{bmatrix} c_{1.xx} & c_{1.xy} \\ c_{1.yx} & c_{1.yy} \end{bmatrix}$	$\begin{bmatrix} 8 \times 10^5 & -1 \times 10^5 \\ -1 \times 10^5 & 10 \times 10^5 \end{bmatrix}$ N·s/m	$\begin{bmatrix} c_{2.xx} & c_{2.xy} \\ c_{2.yx} & c_{2.yy} \end{bmatrix}$	$\begin{bmatrix} 1 \times 10^5 & -1.4 \times 10^5 \\ -1.4 \times 10^5 & 1.5 \times 10^5 \end{bmatrix}$ N·s/m
$\begin{bmatrix} k_{3.xx} & k_{3.xy} \\ k_{3.yx} & k_{3.yy} \end{bmatrix}$	$\begin{bmatrix} 4 \times 10^6 & 7 \times 10^6 \\ -1.6 \times 10^6 & 1.1 \times 10^6 \end{bmatrix}$ N/m	$\begin{bmatrix} k_{4.xx} & k_{4.xy} \\ k_{4.yx} & k_{4.yy} \end{bmatrix}$	$\begin{bmatrix} 4.5 \times 10^6 & 0.9 \times 10^6 \\ -2 \times 10^6 & 1.4 \times 10^6 \end{bmatrix}$ N/m
$\begin{bmatrix} c_{3.xx} & c_{3.xy} \\ c_{3.yx} & c_{3.yy} \end{bmatrix}$	$\begin{bmatrix} 2 \times 10^5 & -1.5 \times 10^5 \\ -1.5 \times 10^5 & 1.6 \times 10^5 \end{bmatrix}$ N·s/m	$\begin{bmatrix} c_{4.xx} & c_{4.xy} \\ c_{4.yx} & c_{4.yy} \end{bmatrix}$	$\begin{bmatrix} 1 \times 10^5 & -2 \times 10^5 \\ -2 \times 10^5 & 2 \times 10^5 \end{bmatrix}$ N·s/m
$\begin{bmatrix} k_{5.xx} & k_{5.xy} \\ k_{5.yx} & k_{5.yy} \end{bmatrix}$	$\begin{bmatrix} 5 \times 10^6 & 1.5 \times 10^6 \\ -2.5 \times 10^6 & 2 \times 10^6 \end{bmatrix}$ N/m	$\begin{bmatrix} k_{6.xx} & k_{6.xy} \\ k_{6.yx} & k_{6.yy} \end{bmatrix}$	$\begin{bmatrix} 3 \times 10^6 & 1 \times 10^6 \\ -1 \times 10^6 & 4 \times 10^6 \end{bmatrix}$ N/m
$\begin{bmatrix} c_{5.xx} & c_{5.xy} \\ c_{5.yx} & c_{5.yy} \end{bmatrix}$	$\begin{bmatrix} 2 \times 10^5 & -3 \times 10^5 \\ -3 \times 10^5 & 3 \times 10^5 \end{bmatrix}$ N·s/m	$\begin{bmatrix} c_{6.xx} & c_{6.xy} \\ c_{6.yx} & c_{6.yy} \end{bmatrix}$	$\begin{bmatrix} 1 \times 10^5 & -0.6 \times 10^5 \\ -0.6 \times 10^5 & 2 \times 10^5 \end{bmatrix}$ N·s/m
$\begin{bmatrix} k_{7.xx} & k_{7.xy} \\ k_{7.yx} & k_{7.yy} \end{bmatrix}$	$\begin{bmatrix} 3 \times 10^6 & 6 \times 10^6 \\ -1.5 \times 10^6 & 1 \times 10^6 \end{bmatrix}$ N/m	$\begin{bmatrix} k_{8.xx} & k_{8.xy} \\ k_{8.yx} & k_{8.yy} \end{bmatrix}$	$\begin{bmatrix} 4 \times 10^6 & 7 \times 10^6 \\ -1.6 \times 10^6 & 1.1 \times 10^6 \end{bmatrix}$ N/m
$\begin{bmatrix} c_{7.xx} & c_{7xy} \\ c_{7.yx} & c_{7.yy} \end{bmatrix}$	$\begin{bmatrix} 4 \times 10^5 & -1.4 \times 10^5 \\ -1.4 \times 10^5 & 1.5 \times 10^5 \end{bmatrix}$ N·s/m	$\begin{bmatrix} c_{8.xx} & c_{8.xy} \\ c_{8.yx} & c_{8.yy} \end{bmatrix}$	$\begin{bmatrix} 7 \times 10^5 & -1.5 \times 10^5 \\ -1.5 \times 10^5 & 16 \times 10^5 \end{bmatrix}$ N·s/m

Table 6. Parameters of the eight rolling bearings in the rotors g1.1, g1.4, and g4.4.

Parameter	Value	Parameter	Value
$\begin{bmatrix} k_{1.xx} & k_{1.xy} \\ k_{1.yx} & k_{1.yy} \end{bmatrix}$	$\begin{bmatrix} 1.8 \times 10^7 & 0 \\ 0 & 1.84 \times 10^7 \end{bmatrix}$ N/m	$\begin{bmatrix} k_{jj.xx} & k_{jj.xy} \\ k_{jj.yx} & k_{jj.yy} \end{bmatrix}, jj = 2 \text{ to } 8$	$\begin{bmatrix} 9 \times 10^6 & 0 \\ 0 & 8.9 \times 10^6 \end{bmatrix}$ N/m
$\begin{bmatrix} c_{1.xx} & c_{1.xy} \\ c_{1.yx} & c_{1.yy} \end{bmatrix}$	$\begin{bmatrix} 75 & 0 \\ 0 & 70 \end{bmatrix}$ N·s/m	$\begin{bmatrix} c_{jj.xx} & c_{jj.xy} \\ c_{jj.yx} & c_{jj.yy} \end{bmatrix}, jj = 2 \text{ to } 8$	$\begin{bmatrix} 80 & 0 \\ 0 & 75 \end{bmatrix}$ N·s/m

3.2. Accuracy of SDA and TODA

3.2.1. Results

(1) Results of the first kind of simulation

Figures 5 and 6 were obtained by using the computational example h1.4 based on SDA and TODA, respectively. They represent the maximum identification errors of each rotor unbalance. In the simulation, #10 point was used as one of the required measuring points and the other measuring points were #3, #47, #11, #21, #31, and #41 points at the location of the two bearings and the four discs. The form $\alpha\% \angle \beta^\circ$, in which $\alpha\%$ is the identification error for the rotor unbalance amplitude and β° represents the identification error for the rotor unbalance angle, is used to express the identification error for rotor unbalance.

According to Figure 5, for SDA, the maximum relative errors of the amplitude of rotor unbalance for #1-#4 discs are almost equal to zero and are $1.70545 \times 10^{-8}\%$, $1.4489 \times 10^{-6}\%$, $3.22562 \times 10^{-5}\%$, and $2.8886 \times 10^{-5}\%$, respectively. For the rotor unbalance angle, the maximum absolute errors, which are $5.5059 \times 10^{-9}^\circ$, $5.99272 \times 10^{-7}^\circ$, $5.83537 \times 10^{-5}^\circ$, and $1.93098 \times 10^{-5}^\circ$, respectively, also equal zero.

According to Figure 6, for TODA, the maximum relative errors of the rotor unbalance amplitude of each disc are $1.14223 \times 10^{-6}\%$, $2.66709 \times 10^{-5}\%$, 0.00102% , and $1.6262 \times 10^{-4}\%$, respectively. The maximum absolute errors of the rotor unbalance angle are $4.68235 \times 10^{-7}^\circ$, $1.59148 \times 10^{-5}^\circ$, $4.41457 \times 10^{-4}^\circ$, and $5.47386 \times 10^{-5}^\circ$, respectively. Although they are bigger than the maximum errors obtained by SDA, they can be also considered equal to zero.

Similar results can be found for the first kind of calculation simulation example for g1.1, h1.1, h4.4, and g1.4, according to Table A1 and Figures A1–A4 in Appendix A.

However, according to Figures 7 and 8, which show the maximum identification errors of each rotor unbalance for g4.4, for TODA, the first two errors are very small, but the maximum identification errors of rotor unbalance for #3 and #4 discs are too big, according to Figure 8. The first two errors are $7.52405 \times 10^{-5}\% \angle 1.81997 \times 10^{-4}^\circ$, $0.17108\% \angle 0.03405^\circ$, while for the errors for #3 and #4 discs, they are $123.71543\% \angle 21.8563^\circ$ and $1281.45771\% \angle 21.69524^\circ$, respectively. Whereas, for SDA, the maximum identification errors of rotor unbalance for #1-#4 discs are $4.70411 \times 10^{-8}\% \angle 1.49579 \times 10^{-7}^\circ$, $5.00642 \times 10^{-4}\% \angle 1.41912 \times 10^{-4}^\circ$, $0.28694\% \angle 0.12378^\circ$, and $0.16497\% \angle 1.57779^\circ$, respectively, according to Figure 8.

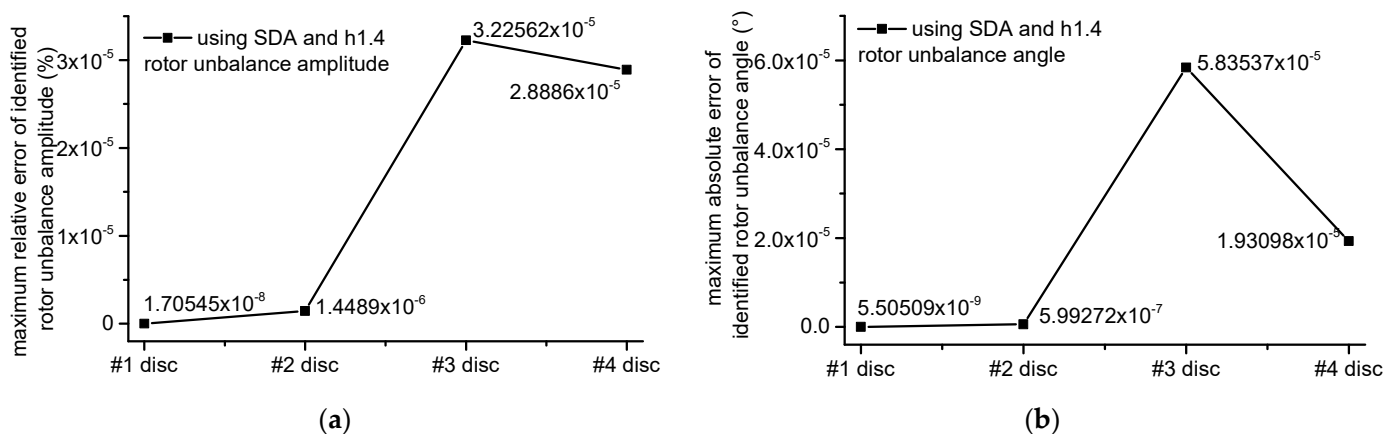


Figure 5. The maximum identification error for each rotor unbalance in h1.4 based on SDA using #10 point as one of the required measuring points: (a) relative error for the rotor unbalance amplitude; (b) absolute error for the rotor unbalance angle.

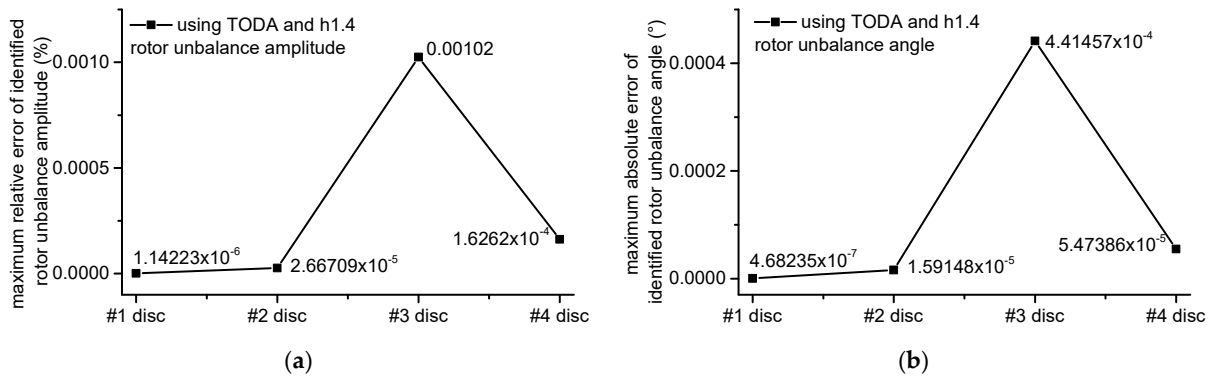


Figure 6. The maximum identification error for each rotor unbalance in h1.4 based on TODA using #10 point as one of the required measuring points: (a) relative error for the rotor unbalance amplitude; (b) absolute error for the rotor unbalance angle.

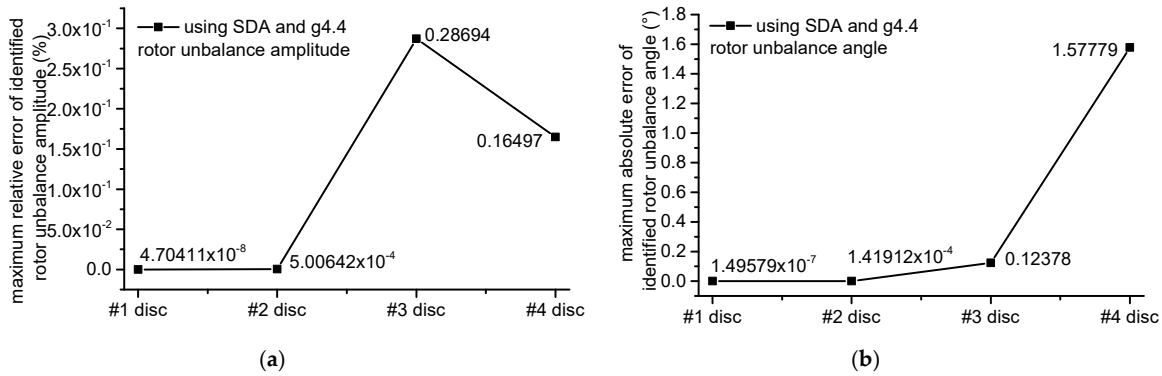


Figure 7. The maximum identification error for each rotor unbalance in g4.4 based on SDA using #20 point as one of the required measuring points: (a) relative error for the rotor unbalance amplitude; (b) absolute error for the rotor unbalance angle.

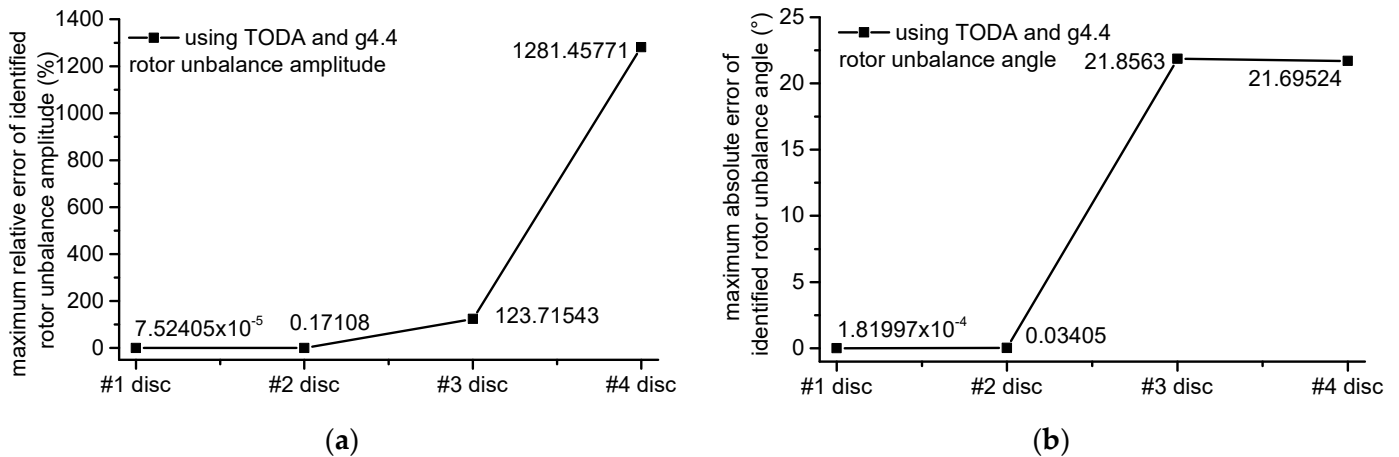


Figure 8. The maximum identification error for each rotor unbalance in g4.4 based on TODA using #20 point as one of the required measuring points: (a) relative error for the rotor unbalance amplitude; (b) absolute error for the rotor unbalance angle.

Moreover, Figure 9 represents the rotor unbalance identification errors for #3 and #4 discs from 1 to 2001 Hz obtained. The maximum identification error for rotor unbalance for #3 disc occurs at 1 Hz. For #4 disc, the maximum identification errors of the rotor unbalance amplitude and angle occur at 1 Hz and 2 Hz, respectively. However, when the rotating frequency becomes high, the identification errors are almost equal to zero.

(2) Results of the second kind of simulation

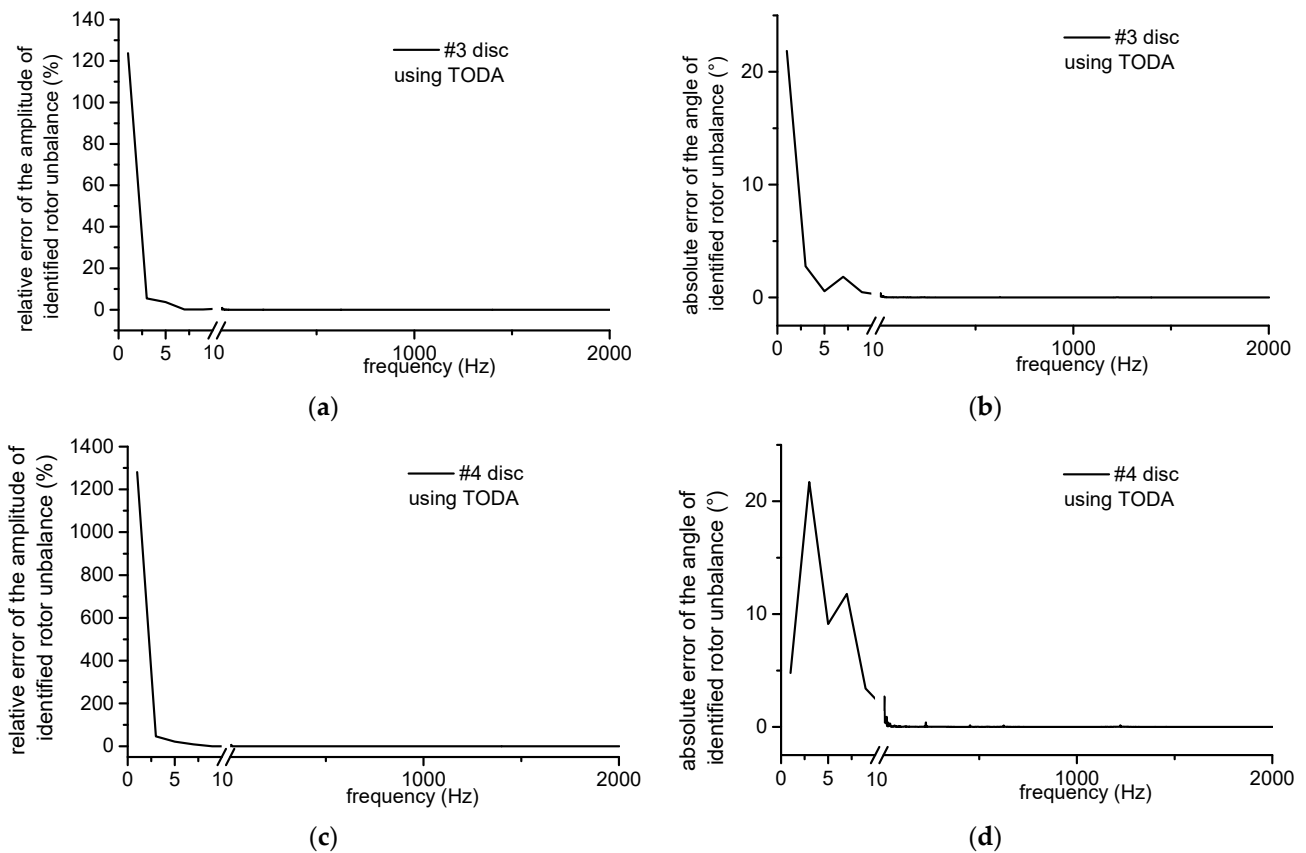


Figure 9. Identification error changed with rotating frequency based on TODA using #20 point as one of the required measuring points in the simulation of g.4.4: (a) rotor unbalance amplitude of #3 disc; (b) rotor unbalance angle of #3 disc; (c) rotor unbalance amplitude of #4 disc; (d) rotor unbalance angle of #4 disc.

Figures 10 and 11, which represent the maximum identification errors of each rotor unbalance for h1.4 are obtained based on SDA and TODA, respectively. In this simulation, #10 point was used as one of the required measuring points and the other measuring points were #3, #47, #11, #21, #31, and #41 at the locations of the two bearings and the four discs.

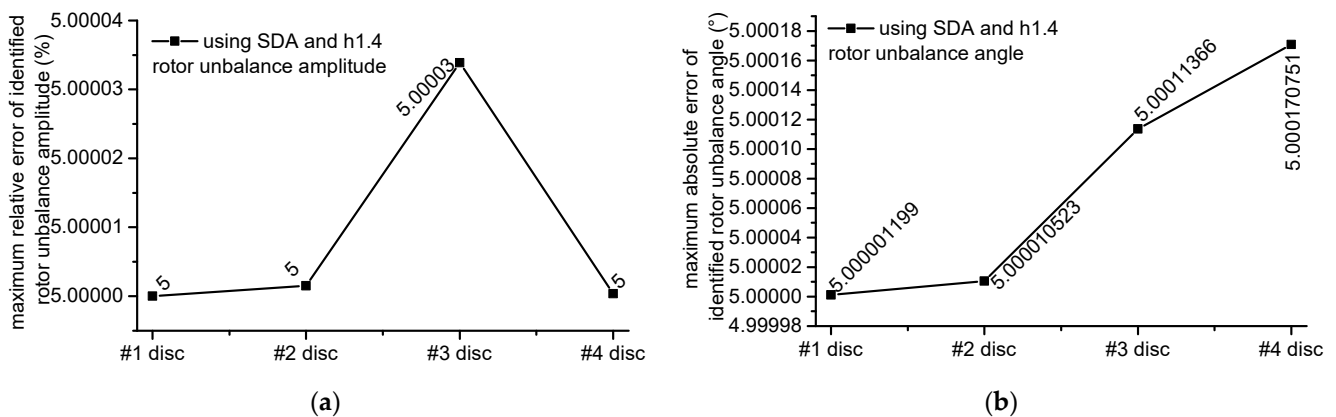


Figure 10. The maximum identification errors of each rotor unbalance in h1.4 based on SDA using #10 point as one of the required measuring points: (a) relative error for the rotor unbalance amplitude; (b) absolute error for the rotor unbalance angle.

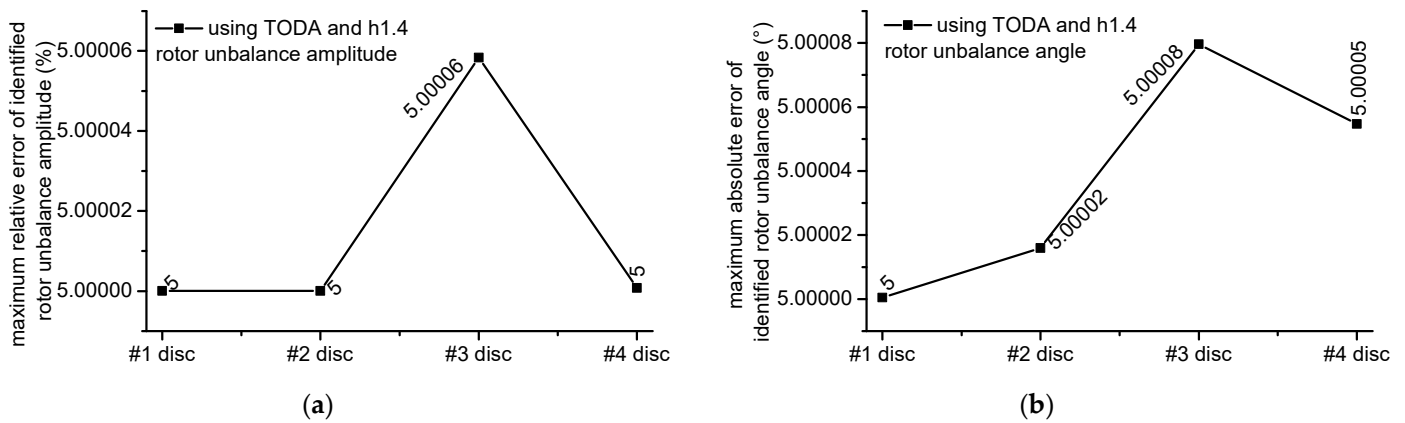


Figure 11. The maximum identification error for each rotor unbalance in h1.4 based on TODA using #10 point as one of the required measuring points (the other measuring points are at the location of the two bearings and the four discs): (a) relative error for the rotor unbalance amplitude; (b) absolute error for the rotor unbalance angle.

According to Figure 10, for SDA, the maximum relative errors of the rotor unbalance for #1–#4 discs are $5\% \angle 5.000001199^\circ$, $5\% \angle 5.000020523^\circ$, $5.00003\% \angle 5.00022366^\circ$, and $5\% \angle 5.000170751^\circ$, respectively, which are almost equal to the setting errors ($5\% \angle 5^\circ$) of the inputted unbalance responses. According to Figure 11, for TODA, the maximum relative errors of rotor unbalance for each disc also almost equal the setting error. They are $5\% \angle 5^\circ$, $5\% \angle 5.00002^\circ$, $5.00006\% \angle 5.00008^\circ$, and $5\% \angle 5.00005^\circ$, respectively. Similar results can be found in the second kind of calculation simulation example for g1.1, h1.1, h4.4, and g1.4, according to Table A2 and Figures A5–A8 in Appendix B.

However, according to Figures 12 and 13, which show the maximum identification errors of each rotor unbalance for g4.4, for TODA, the maximum identification errors of rotor unbalance for #3 and #4 discs are $134.9012142\% \angle 16.8563^\circ$ and $1350.530732\% \angle 26.69523^\circ$, respectively, although the errors for #1 and #2 discs are almost equal the setting error $5\% \angle 5^\circ$. Whereas, for SDA, the maximum identification errors for the rotor unbalance for #1–#4 discs are $5\% \angle 5^\circ$, $5.00001\% \angle 5.00014^\circ$, $5.0039\% \angle 5.00404^\circ$, and $5.17322\% \angle 6.57779^\circ$, respectively. Only the rotor unbalance angle of #4 disc is a bit bigger than the setting error of 5%. The others are almost equal to the input setting error of $5\% \angle 5^\circ$.

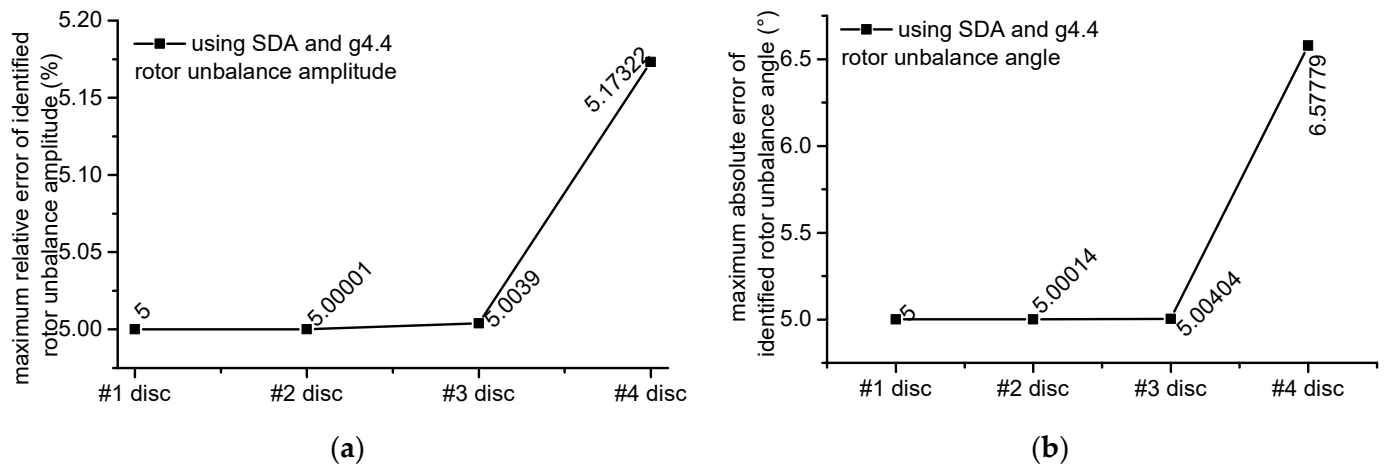


Figure 12. The maximum identification error for each rotor unbalance in g4.4 based on SDA using #20 point as one of the required measuring points: (a) relative error for the rotor unbalance amplitude; (b) absolute error for the rotor unbalance angle.

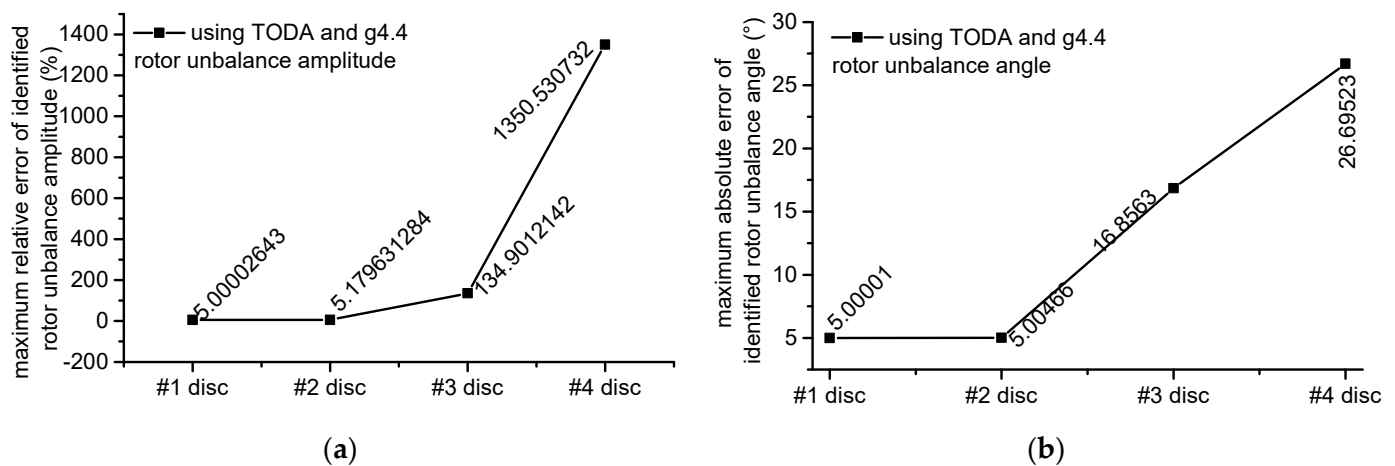


Figure 13. The maximum identification error for each rotor unbalance in g4.4 based on TODA using #20 point as one of the required measuring points (the other measuring points are at the location of the two bearings and the four discs): (a) relative error for the rotor unbalance amplitude; (b) absolute error for the rotor unbalance angle.

Hence, the rotor unbalance identification errors for #3 and #4 discs from 1 to 2001 Hz are as shown in Figure 14. The maximum error occurs at the beginning. The maximum identification error for rotor unbalance for #3 disc is at 1 Hz. For #4 disc, the maximum identification errors of rotor unbalance amplitude and angle are at 1 Hz and 2 Hz, respectively. However, when the rotating frequency becomes high, the identification errors are almost equal the input setting error of 5%∠5°.

3.2.2. Discussion

In the first kind of numerical simulation, the simulated unbalance responses calculated by the CRDAM were fed into SDA and TODA to estimate the rotor unbalance. For SDA, the identified rotor unbalance was equal to the set value of rotor unbalance. For TODA, the identified rotor unbalance was equal to the set value of rotor unbalance except for the simulation of g4.4. The error for the identified rotor unbalance for #3 and #4 discs in g4.4 is big at the low rotating frequency (1 Hz, 2 Hz) but very small at other rotating frequencies.

In the second kind of numerical simulation, the simulated unbalance responses, which were calculated by the CRDAM and contaminated the set measured error (5%, 5°), were fed into SDA and TODA. For SDA, the identified error was equal to the set error. For TODA, the identified rotor unbalance was almost equal to the set error except for the simulation of g4.4. The error for the identified rotor unbalance for #3 and #4 discs in g4.4 was bigger than the set errors at the low rotating frequency (1 Hz, 2 Hz) but almost equal to the set error at other frequencies.

The unbalance responses in both the x and y directions were needed when using TODA. At a low frequency, the value of the unbalance response is very small. The errors in computer calculations, such as rounding errors, have a considerable influence on small values. Accordingly, there were errors with regard to the unbalance responses in both the x and y directions at low frequencies. If the errors in the x and y directions are quite different, a big identification error may occur at a low frequency for TODA because the errors in the x direction are divided by the errors in the y direction, while, for SDA, the unbalance response in only one direction is needed. Hence, the identification error can be equal to the set measured error.

Therefore, the error for the identified rotor unbalance response will be equal to the set error if the errors of all the measured unbalance responses are the same. It is indicated that the repeatability precision of each measuring channel of the unbalance response measurement system plays a critical role when it comes to using the proposed algorithms. In engineering, the vibration caused by rotor unbalance can be very small for low-speed

rotors and the measuring system cannot accurately detect tiny vibrations. Therefore, the proposed method, especially TODA, cannot be applied to low-speed rotors.

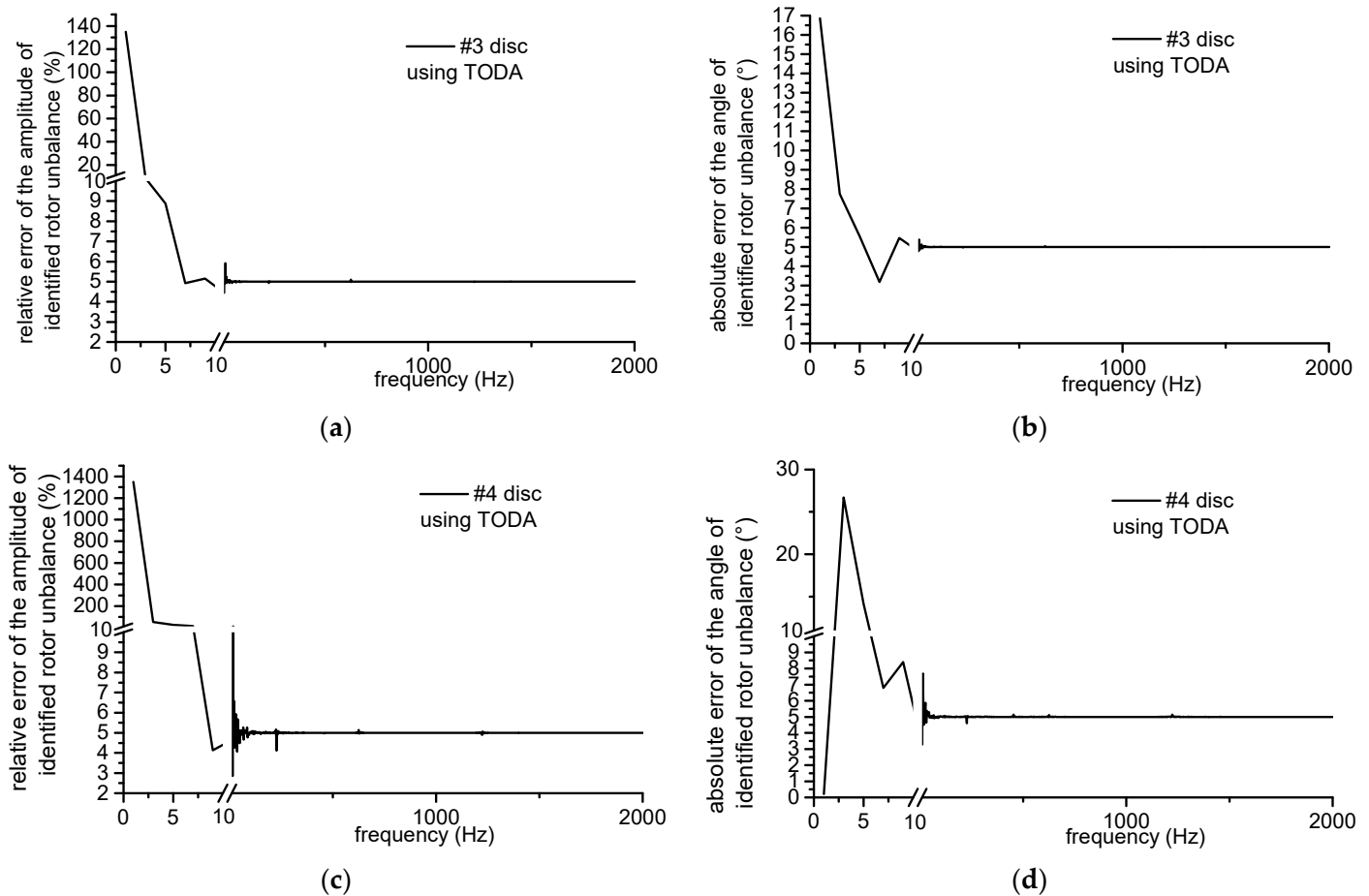


Figure 14. Identification error changed with rotating frequency based on TODA using #20 point as one of the required measuring points in the simulation for g.4.4: (a) rotor unbalance amplitude of #3 disc; (b) rotor unbalance angle of #3 disc; (c) rotor unbalance amplitude of #4 disc; (d) rotor unbalance angle of #4 disc.

3.3. Adjustment Point

3.3.1. Results

In the third kind of simulation of g1.4, the matrix of the maximum identified error for rotor unbalance for each disc was obtained with Equations (24)–(27). The numbers of AFPs were also obtained. They are shown in Figures 15–18. The simulations were conducted by using simulated unbalance responses as input data to SDA and TODA and by changing one measuring point which was close to the identified disc. The #20, #40, #60, and #80 points were used for the respective changes. The other $m + n$ measuring points were at the discs and bearings. The simulated unbalance responses were calculated by means of the CRDAM contaminating the sensor resolution at 0.1 nm.

In Equations (24)–(27), the four element values in a row of the matrix are the maximum identification errors of unbalance for #1–#4 discs, respectively, when using the same measuring point. The four elements in a column are the maximum identification errors of unbalance for the same disc when the measuring points #20, #40, #60, and #80 were applied, respectively. By comparing the biggest identification error obtained under different adjustment point conditions when the rotating frequency is changed from 1 to 2001 Hz, it is easy to find that the adjustment point plays a critical role in improving the identification accuracy for SDA and TODA. The details are as follows:

- (1) According to Equations (24) and (25), for SDA, when #20 point, which is near #1 disc, is used as one of the required measuring points, the maximum identification error for rotor unbalance for #1 disc is the smallest among that of the four discs. The maximum identification error for rotor unbalance is $10.84\% \angle 2.12^\circ$, while for #2–4 discs, their maximum errors are much bigger. When #40 point, which is close to #2 disc is used, the maximum identification error for rotor unbalance for #2 disc becomes the smallest. It is $42.54\% \angle 8.60^\circ$. When #60 point, which is beside #3 disc, is used, #3 disc’s rotor unbalance identification error, which is $257.24\% \angle 57.41^\circ$, is the second smallest and is close to the smallest error of $254.72\% \angle 51.14^\circ$. When #80 point, which is beside #4 disc, is used, #4 disc’s rotor unbalance identification error, which is $9.82\% \angle 16.25^\circ$, is much smaller than the others. From the perspective of the column in the matrix, when the measuring point is changed from #20 to #40, the maximum identification error for rotor unbalance for #1 disc becomes bigger, while the maximum identification error for rotor unbalance for #4 disc becomes smaller. The maximum identification errors for rotor unbalance for #2 and #3 discs are also changed apparently. As #20 point is applied, #1 disc acquires the best recognition accuracy, while #2 disc has the best recognition accuracy as #40 point is applied, #3 disc has the best recognition accuracy as #60 point is applied, and #4 disc has the best recognition accuracy as #80 point is applied.
- (2) As for TODA, similar results can be obtained, although the values of maximum identification errors are much bigger than the maximum identification errors for SDA, according to Equations (26) and (27). When #20 point, which is near #1 disc, is used as one of the required measuring points, the maximum identification error for rotor unbalance for #1 disc is the smallest among that of the four discs. The maximum identification error for rotor unbalance is $4.22 \times 10^2\% \angle 170.38^\circ$, while for #2–4 disc, their maximum errors are much bigger. When #40 point, which is close to #2 disc, is used, the maximum identification error for rotor unbalance for #2 disc becomes the smallest. It is $1.64 \times 10^4\% \angle 140.73^\circ$. When #60 point, which is beside #3 disc, is used, #3 disc’s rotor unbalance identification error, which is $6.03 \times 10^4\% \angle 179.57^\circ$, is the second smallest. When #80 point, which is beside #4 disc, is used, #4 disc’s rotor unbalance identification error is $2.68 \times 10^{15}\% \angle 179.95^\circ$. Although it is the biggest among the obtained maximum identification errors of the four discs, it is the smallest error for #4 disc, which can be obtained by changing the measuring point from #20 to #40. From the perspective of the column in the matrix, when the measuring point is changed from #20 to #40, the maximum identification error for rotor unbalance for #1 disc becomes bigger. The maximum identification errors of rotor unbalance for #2, #3, and #4 discs are also changed apparently. As #20 point is applied, #1 disc acquires the best recognition accuracy, while #2 disc has the best recognition accuracy as #40 point is applied, #3 disc has the best recognition accuracy of unbalance amplitude as #60 point is applied, and #4 disc has the best recognition accuracy as #80 point is applied.

$$SDA_M1_{g14} = \begin{bmatrix} 10.84 & 376.18 & 14934.67 & 22570.13 \\ 400.78 & 42.54 & 7251.41 & 4823.78 \\ 382.89 & 254.72 & 257.54 & 3203.79 \\ 1153.90 & 475.79 & 1148.01 & 9.82 \end{bmatrix} \quad (24)$$

$$SDA_M2_{g14} = \begin{bmatrix} 2.12 & 152.05 & 179.19 & 170.46 \\ 83.28 & 8.60 & 178.20 & 173.14 \\ 132.99 & 51.14 & 57.41 & 173.82 \\ 121.58 & 141.59 & 139.37 & 16.25 \end{bmatrix} \quad (25)$$

$$TODA_M1_{g14} = \begin{bmatrix} 4.22 \times 10^2 & 1.54 \times 10^5 & 1.04 \times 10^7 & 7.39 \times 10^{18} \\ 4.97 \times 10^4 & 1.46 \times 10^4 & 3.45 \times 10^6 & 9.50 \times 10^{17} \\ 3.66 \times 10^4 & 6.58 \times 10^4 & 6.03 \times 10^4 & 1.37 \times 10^{17} \\ 9.14 \times 10^5 & 1.94 \times 10^6 & 3.89 \times 10^6 & 2.68 \times 10^{15} \end{bmatrix} \quad (26)$$

$$TODA_M2_{g14} = \begin{bmatrix} 170.38 & 179.83 & 178.53 & 179.98 \\ 178.23 & 140.73 & 179.01 & 180.00 \\ 179.27 & 179.76 & 179.57 & 179.99 \\ 179.75 & 179.67 & 179.67 & 179.95 \end{bmatrix} \quad (27)$$

where SDA_M1_{g14} and SDA_M2_{g14} are the matrix of the maximum identification error for rotor unbalance amplitude and the angle of #1 to #4 discs under different adjustment point conditions using SDA; $TODA_M1_{g14}$ and $TODA_M2_{g14}$ are the matrix of the maximum identification error for rotor unbalance amplitude and the angle of #1 to #4 discs under different adjustment point conditions using TODA.

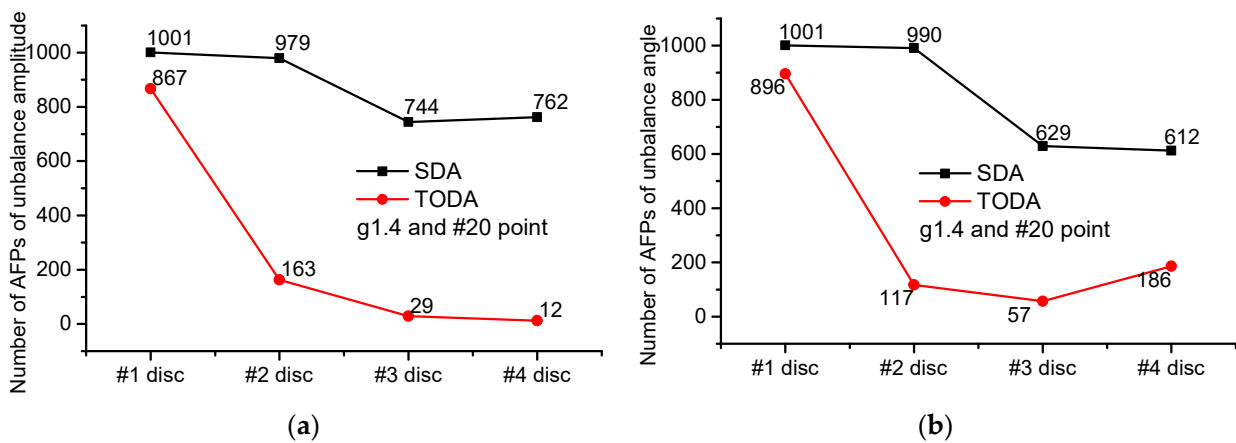


Figure 15. Statistical results of the number of AFPs of rotor unbalance for each disc in the simulation of g1.4 using #20 point as one of the required measuring points and using a 0.1 nm resolution: (a) results for the unbalance amplitude; (b) results for the unbalance angle.

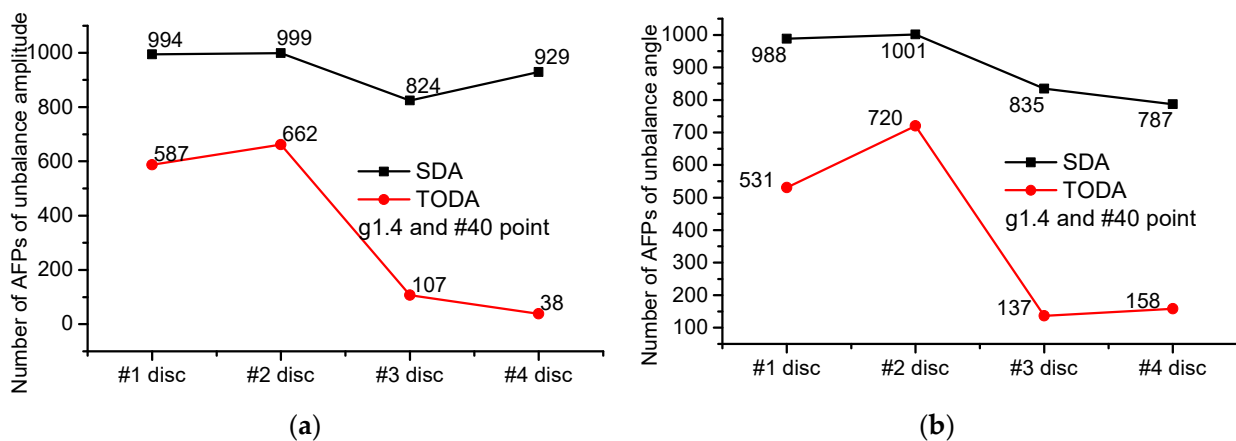


Figure 16. Statistical results of the number of AFPs of rotor unbalance for each disc in the simulation of g1.4 using #40 point as one of the required measuring points and using a 0.1 nm resolution: (a) results for the unbalance amplitude; (b) results for the unbalance angle.

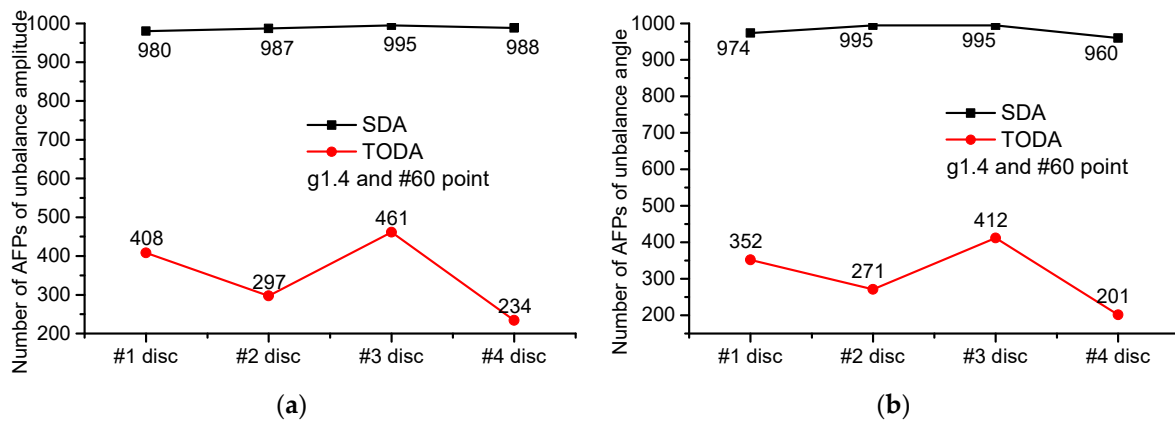


Figure 17. Statistical results of the number of AFPs of rotor unbalance for each disc in the simulation of g1.4 using #60 point as one of the required measuring points and using a 0.1 nm resolution: (a) results for the unbalance amplitude; (b) results for the rotor unbalance angle.

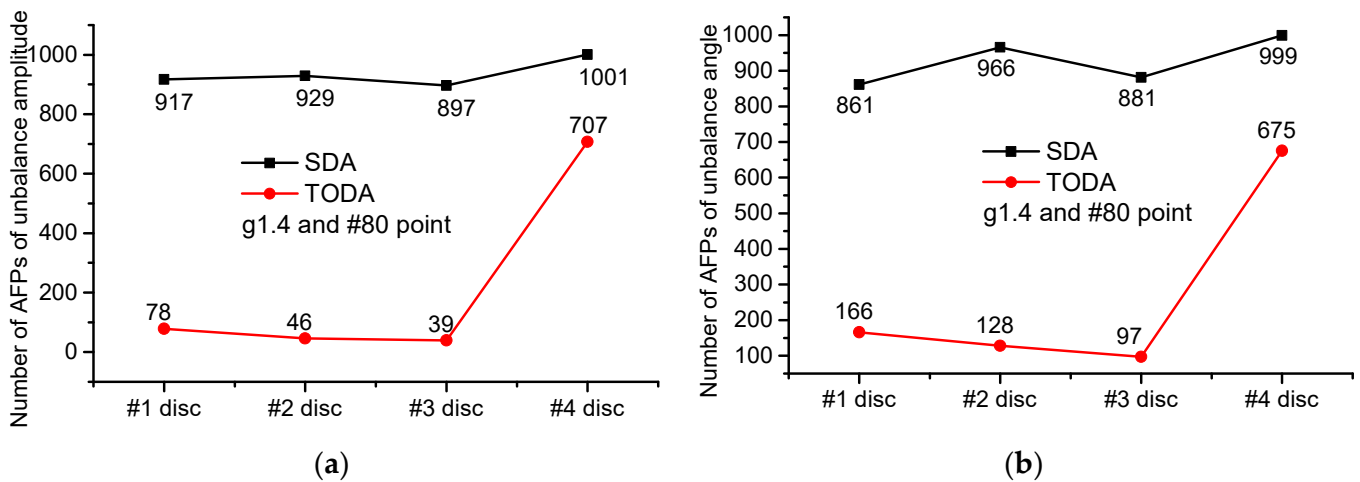


Figure 18. Statistical results of the number of AFPs of rotor unbalance for each disc in the simulation of g1.4 using #80 point as one of the required measuring points and using a 0.1 nm resolution: (a) results for the unbalance amplitude; (b) results for the unbalance angle.

According to the number of AFPs of rotor unbalance obtained by SDA in Figures 15–18, the results are as follows:

- (1) The numbers of AFPs of rotor unbalance amplitude for #1–#4 discs are 1001, 979, 744, and 762, respectively, according to Figure 15a. For the rotor unbalance angle, there are 1001, 990, 629, and 612 AFPs, respectively, according to Figure 15b. This indicates that the identification results for rotor unbalance for #1 disc are best when #20 point is used as one of the required measuring points.
- (2) According to Figure 16, there are 994, 999, 824, and 929 AFPs, respectively, for the rotor unbalance amplitude of #1 disc, #2 disc, #3 disc, and #4 disc, and 988, 1001, 835, and 787 AFPs, respectively, for the rotor unbalance angle. This indicates that the identification results for rotor unbalance for #2 disc are best when #40 point is used as one of the required measuring points.
- (3) According to Figure 17, the numbers of AFPs of rotor unbalance amplitude are 980, 987, 995, and 988, respectively, and the numbers of rotor unbalance angles are 974, 995, 995, and 960 respectively. This indicates that the identification results for rotor unbalance for #3 disc are best when #60 point is used as one of the required measuring points.

- (4) According to Figure 18, for the rotor unbalance amplitude of #1 disc, #2 disc, #3 disc, and #4 disc, there are 917, 929, 897, and 1001 AFPs, respectively. For the angle, there are 861, 966, 881, and 999 AFPs, respectively. This indicates that the identification results for rotor unbalance for #4 disc are best when #80 point is used as one of the required measuring points.

For TODA, the same conclusion can be obtained according to Figures 15–18, although the number of AFPs obtained by TODA is obviously lesser than that of SDA. When #20 point is used as one of the required measuring points, the numbers of AFPs of rotor unbalance amplitude for #1–#4 discs are 867, 163, 29, and 12, respectively. For the rotor unbalance angle, there are 896, 117, 57, and 186 AFPs, respectively. Apparently, #1 disc has the most AFPs. When #40 point is used, the numbers of AFPs of rotor unbalance amplitude for #1–#4 discs are 587, 662, 107, and 38, respectively. For the rotor unbalance angle, there are 541, 720, 137, and 158 AFPs, respectively. Apparently, #2 disc has the most AFPs. When #60 point is used, the number of AFPs of rotor unbalance amplitude of #1–#4 discs are 408, 297, 461, and 234, respectively. For the rotor unbalance angle, there are 352, 271, 421, and 201 AFPs, respectively. Obviously, #3 disc has the most AFPs. When #80 point is used, the number of AFPs of rotor unbalance amplitude of #1–#4 discs are 78, 48, 39, and 707, respectively. For the rotor unbalance angle, there are 166, 128, 97, and 675 AFPs, respectively. Obviously, #4 disc has the most AFPs.

Similar results can be found in the third kind of calculation simulation example for g4.4, h1.4, and h4.4, according to Equations (A1)–(A12) and Figures A9–A20 in Appendix C. However, for h4.4, no result can be obtained based on SDA and TODA from 1 Hz to 20 Hz.

3.3.2. Discussion

In the third kind of numerical simulation, the highest sensor resolution (0.1 nm) at present is considered. In the simulation of g1.4 and g4.4, when #20 point, which is near #1 disc, is used as one of the required measuring points, the identification accuracy for the rotor unbalance for #1 disc (at location of #21 point) is high. Similarly, #2 disc at #41 point, #3 disc at #61 point, and #4 disc at #81 point can obtain high identification accuracy for rotor unbalance as #40, #60, and #80 points are used respectively. In the simulation of h1.4 and h4.4, #1 disc at #11 point, #2 disc at #21 point, #3 disc at #31 point, and #4 disc at #41 point can obtain a high identification accuracy for rotor unbalance as #10, #20, #30, and #40 points are used, respectively.

From the above, to obtain good identification results, there should be a measuring point near the disc, for which the rotor unbalance should be identified. The measuring point near the disc determines the identification error for the rotor unbalance and it should be near the disc the unbalance of which is to be identified. Hence, the measuring point is called an adjustment point.

By applying the proposed adjustment point, the identification errors for rotor unbalance for #3 and #4 discs in the first and second kind of simulations are reduced and Figures 19 and 20 are obtained. According to Figure 19, the maximum identification error is almost equal to zero. It is $0.00358\% \angle 0.00193^\circ$ for #3 disc and $2.04046 \times 10^{-4}\% \angle 5.84276 \times 10^{-5}^\circ$ for #4 disc, while they are $123.71543\% \angle 21.8563^\circ$ and $1281.45771\% \angle 21.69524^\circ$, respectively, before the application of the adjustment point. According to Figure 20, the ultimate error is $5.0006\% \angle 5.00193^\circ$ for #3 disc and $4.99979\% \angle 5.00377^\circ$ for #4 disc. They are almost equal to the setting error of $5\% \angle 5^\circ$, while they are $134.9012142\% \angle 16.8563^\circ$ and $1350.530732\% \angle 26.69523^\circ$, respectively, before the application of the adjustment point. Therefore, there should be a sensor mounted near each disc if the unbalances of all the discs are to be identified.

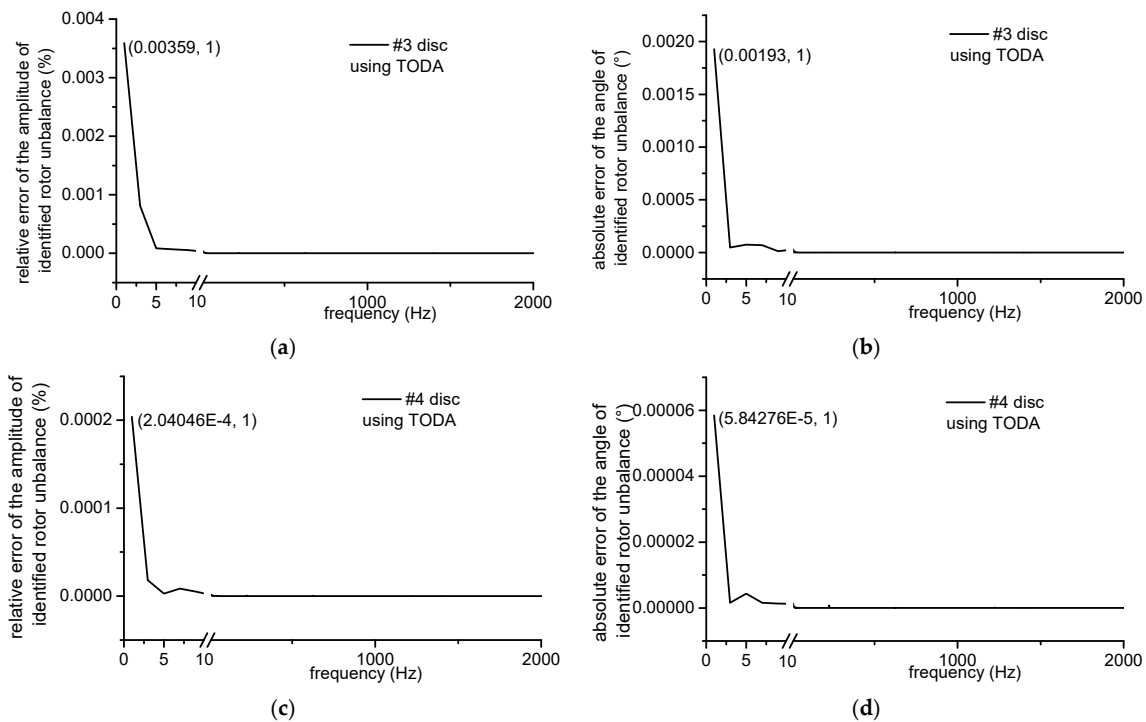


Figure 19. Identification error changed with frequency based on TODA for the first kind of g.4.4 simulation in which the proposed adjustment points (#60 and #80 points) are applied: (a) rotor unbalance amplitude of #3 disc; (b) rotor unbalance angle of #3 disc; (c) rotor unbalance amplitude of #4 disc; (d) rotor unbalance angle of #4 disc.

It was established that SDA has a much better identification accuracy than TODA. The reason is that the unbalance responses in both the x and y directions are involved in TODA and the unbalance response in only one direction is needed for SDA. This means that the measured errors of unbalance responses in both the x and y directions will contribute to the identification error of TODA. Moreover, they are combined by division in TODA. When the measured errors in the two directions are not the same and the error, whose value is smaller, happens to be the denominator, a high identification error occurs. Based on the simulation results, the value of the denominator is smaller in most cases, but the value of the denominator can be bigger, in which case the identification error of SDA is bigger than that of TODA, according to Figures A9, A17 and A20. Moreover, according to Figures A9, A17 and A20, similar results for SDA and TODA can be obtained when the comprehensive effect of the response measuring errors in the x and y directions is equal to that in the x or y direction. It is indicated that the identification result of TODA is greatly affected by the measured error for the unbalance response due to the unbalance responses in both the x and y directions being required. In practical engineering, it is difficult to obtain completely consistent measurement errors for each unbalance response. The measured errors for unbalance responses in the x direction are different from those in the y direction. This may lead to big identification errors for TODA. Hence, SDA is better than TODA from the perspective of engineering applications.

3.4. Affect of Sensor Resolution

3.4.1. Results

According to the result in the third kind of simulation, the maximum identification error of TODA was too big. Hence, the fourth kind of simulation was conducted based on SDA. The simulated unbalance responses calculated by CRDAM containing different sensor resolutions (0.1 nm, 1 nm, 0.1 μ m, and 1 μ m) were used as input data to the method. The computational example g1.4 is used. In the simulation, the measuring points for the

two discs and the four bearings are utilized and #20, #40, #60, and #80 points are used as the respective adjustment points in order to obtain good identification results.

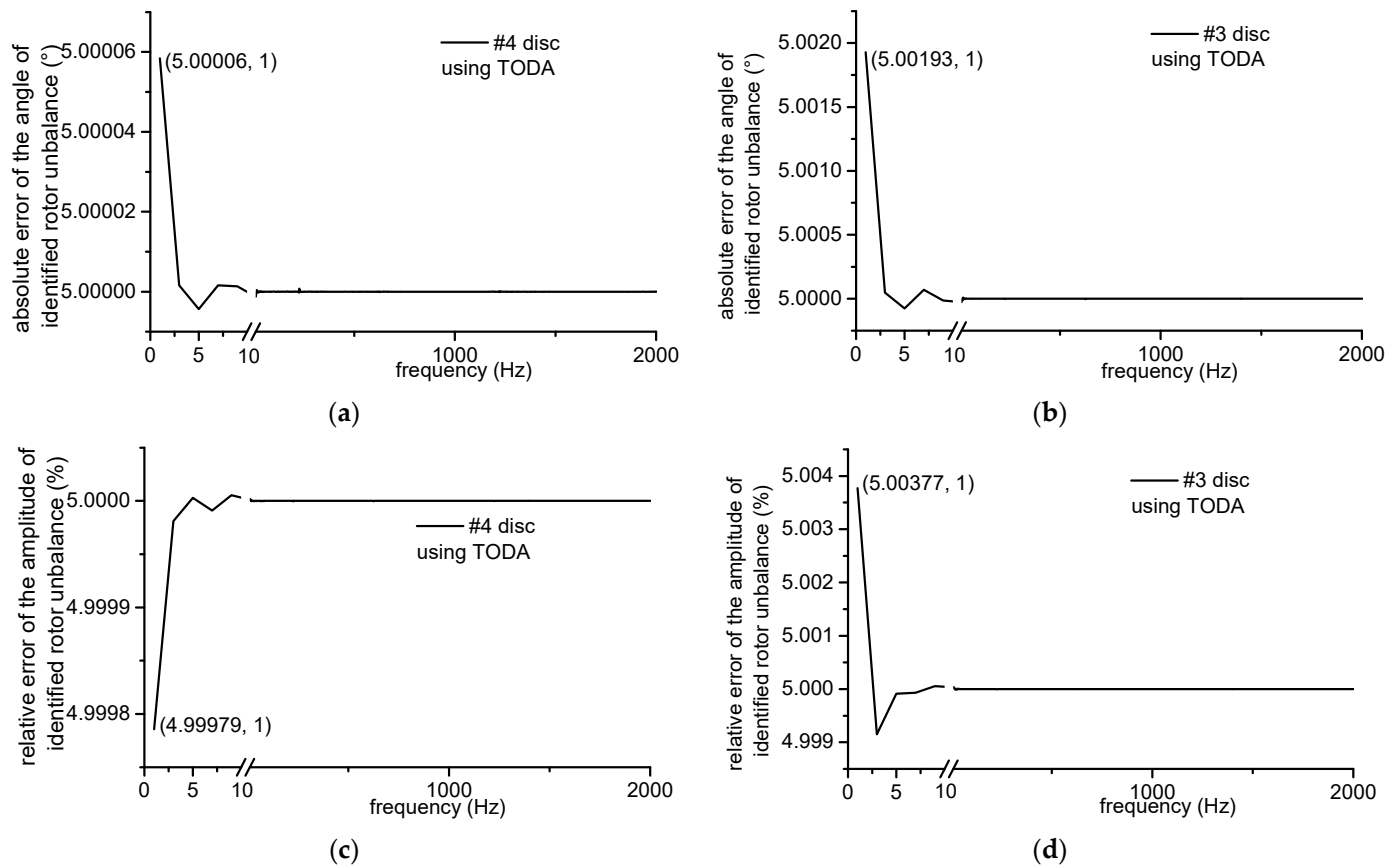


Figure 20. Identification error changed with frequency based on TODA for the second kind of g.4.4 simulation in which the proposed adjustment points (#60 and #80 points) are applied: (a) rotor unbalance amplitude of #3 disc; (b) rotor unbalance angle of #3 disc; (c) rotor unbalance amplitude of #4 disc; (d) rotor unbalance angle of #4 disc.

The curves for the identification errors, which were obtained when the sensor resolutions were 0.1 nm, 1 nm, 0.1 μm , and 1 μm , are shown in Figures 21–24. According to the figures, the identified rotor unbalance changes with the rotating frequencies and there are several peak values for the identified rotor unbalance. The results are as follows:

(1) Sensor resolution of 0.1 nm

According to Figure 21, for #1 disc, the peak values of the amplitude of the identified rotor unbalance are 10.84%, 2.02%, 0.31%, and 0.42% at frequencies of 1 Hz, 271 Hz, 643 Hz, and 1267 Hz, respectively. The peak values of the absolute error for the angle are 2.12° , 1.47° , 0.32° , and 0.32° at 1 Hz, 271 Hz, 645 Hz, and 1267 Hz, respectively.

For #2 disc, the peak values of the amplitude of the identified rotor unbalance are 3.46%, 42.54%, 4.33%, and 1.42% at frequencies of 1 Hz, 269 Hz, 645 Hz, and 1263 Hz, respectively. The peak values of the absolute error for the angle are 2.29° , 8.6° , 0.31° , and 0.8° at 1 Hz, 267 Hz, 645 Hz, and 1265 Hz, respectively.

For #3 disc, the peak values of the amplitude of identified rotor unbalance are 26.02%, 257.24%, 11.64%, and 20.64% at frequencies of 1 Hz, 269 Hz, 645 Hz, and 1265 Hz, respectively. The peak values of the absolute error for the angle are 19.49° , 57.41° , 11.72° , and 7.76° at 1 Hz, 271 Hz, 645 Hz, and 1267 Hz, respectively.

For #4 disc, the peak values of the amplitude of identified rotor unbalance are 9.82%, 6.46%, 0.82%, 0.56%, and 7.61% at frequencies of 1 Hz, 267 Hz, 645 Hz, 809 Hz, and 1267 Hz,

respectively. The peak values of the absolute error for the angle are 16.259° , 1.88° , 1.39° , and 4.15° at 269 Hz, 645 Hz, 809 Hz, and 1265 Hz, respectively.

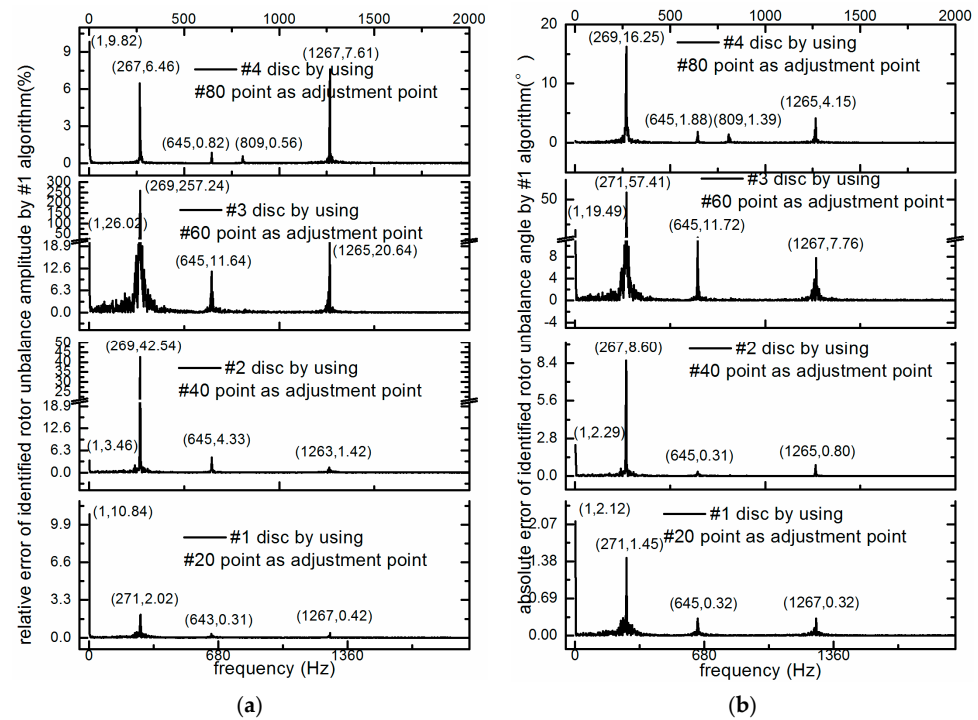


Figure 21. Identified rotor unbalance changing with frequency in g1.4 using a 0.1 nm resolution: (a) obtained rotor unbalance amplitude; (b) obtained rotor unbalance angle.

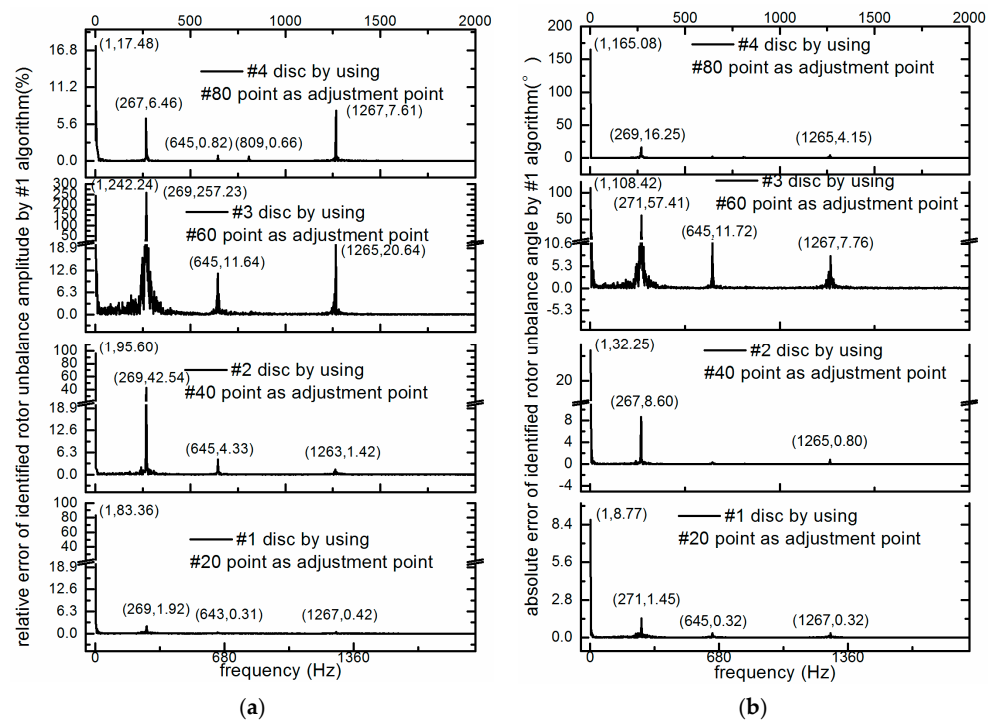


Figure 22. Identified rotor unbalance changing with frequency in g1.4 using a 1 nm resolution: (a) obtained rotor unbalance amplitude; (b) obtained rotor unbalance angle.

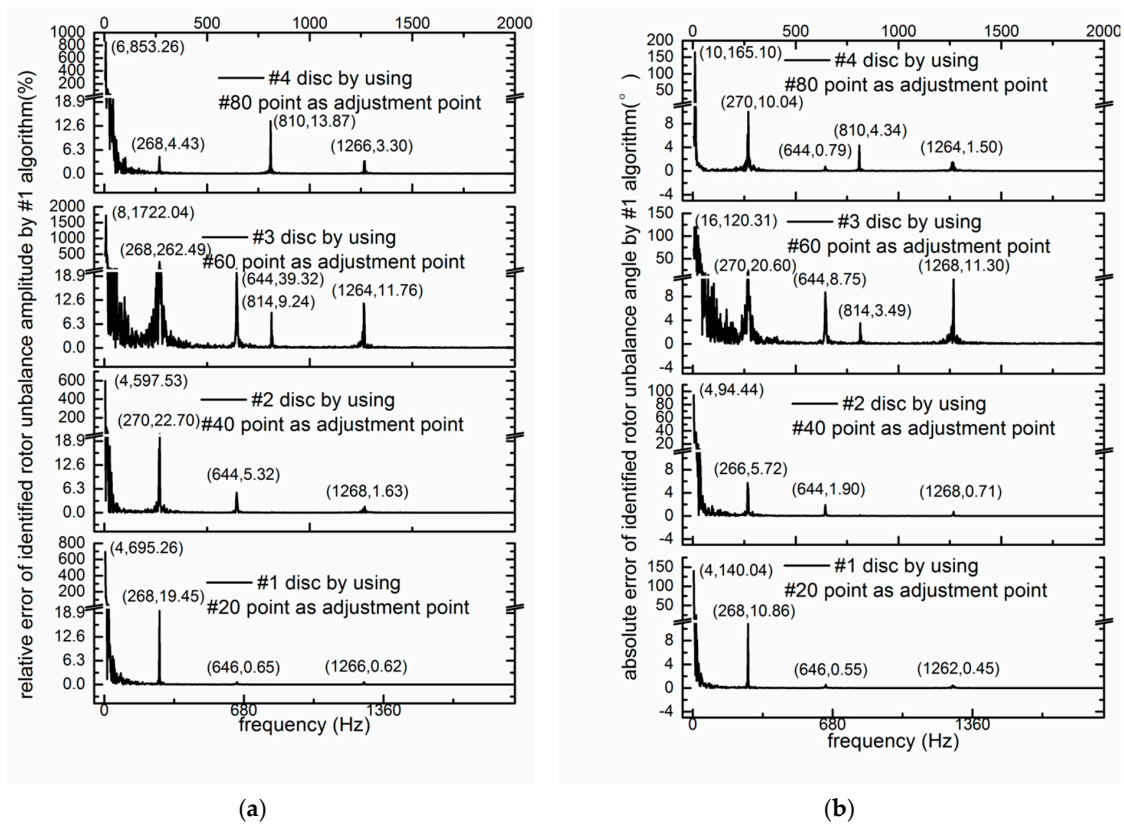


Figure 23. Identified rotor unbalance changing with frequency in g1.4 using a 0.1 um resolution: (a) obtained rotor unbalance amplitude; (b) obtained rotor unbalance angle.

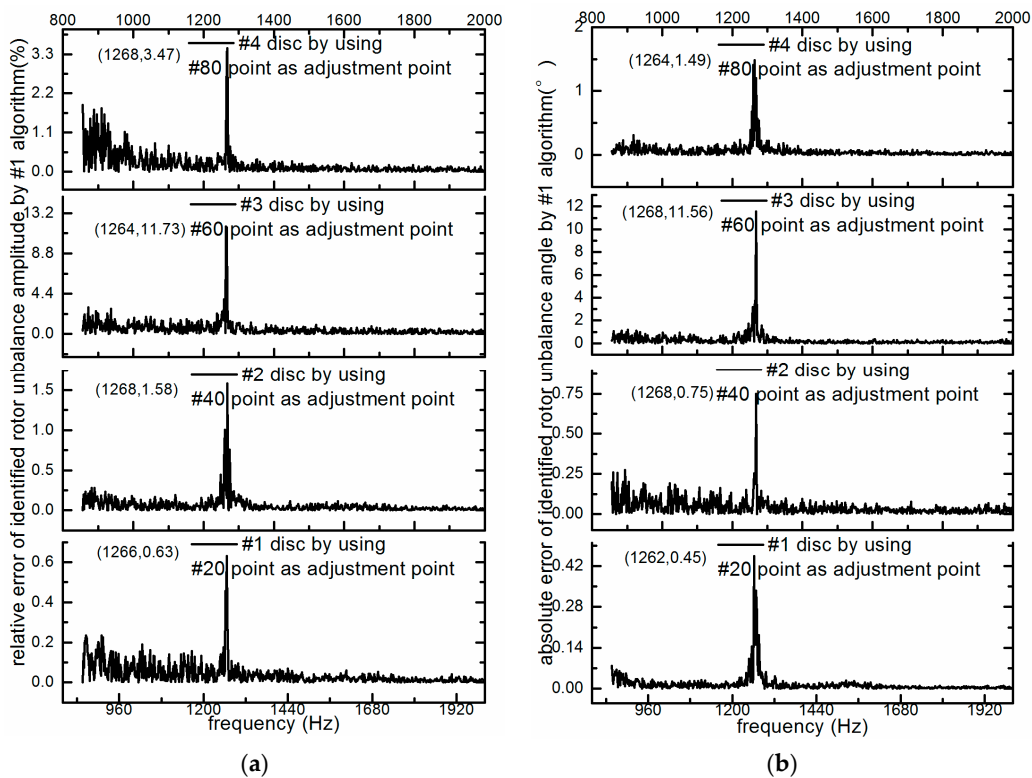


Figure 24. Identified rotor unbalance with frequency in g1.4 using a 1 um resolution: (a) obtained rotor unbalance amplitude; (b) obtained rotor unbalance angle.

(2) Sensor resolution of 1 nm

According to Figure 22, for #1 disc, the peak values of the amplitude of identified rotor unbalance are 83.36%, 1.92%, 0.31%, and 0.42% at frequencies of 1 Hz, 269 Hz, 643 Hz, and 1267 Hz, respectively. The peak values of the absolute error for the angle are 8.77°, 1.45°, 0.32°, and 0.32° at 1 Hz, 271 Hz, 645 Hz, and 1267 Hz, respectively.

For #2 disc, the peak values of the amplitude of identified rotor unbalance are 95.6%, 42.54%, 4.33%, and 1.42% at frequencies of 1 Hz, 269 Hz, 645 Hz, and 1263 Hz, respectively. The peak values of the absolute error for the angle are 32.5°, 8.6°, and 0.8° at 1 Hz, 267 Hz, and 1265 Hz, respectively.

For #3 disc, the peak values of the amplitude of identified rotor unbalance are 242.24%, 257.23%, 11.64%, and 20.64% at frequencies of 1 Hz, 269 Hz, 645 Hz, and 1265 Hz, respectively. The peak values of the absolute error for the angle are 108.42°, 57.41°, 11.72°, and 7.76° at 1 Hz, 271 Hz, 645 Hz, and 1267 Hz, respectively.

For #4 disc, the peak values of the amplitudes of identified rotor unbalance are 17.48%, 6.46%, 0.82%, 0.66%, and 7.61% at frequencies of 1 Hz, 267 Hz, 645 Hz, 809 Hz, and 1267 Hz, respectively. The peak values of the absolute error for the angle are 165.08°, 16.25°, and 4.15° at 1 Hz, 269 Hz, and 1265 Hz, respectively.

(3) Sensor resolution of 0.1 um

With the sensor resolution being reduced to 0.1 um, the minimum starting frequency of the identification was 4 Hz (SDA does not work at a low frequency). According to Figure 23, the results are as follows:

For #1 disc, the peak values of the amplitude of identified rotor unbalance are 695.26%, 19.45%, 0.65%, and 0.62% at frequencies of 4 Hz, 268 Hz, 646 Hz, and 1266 Hz, respectively. The peak values of the absolute error for the angle are 140.04°, 10.86°, 0.55° and 0.45° at 4 Hz, 268 Hz, 646 Hz and 1262 Hz, respectively.

For #2 disc, the peak values of the amplitude of identified rotor unbalance are 597.53%, 22.7%, 5.32% and 1.63% at frequencies of 4 Hz, 270 Hz, 644 Hz, and 1268 Hz, respectively. The peak values of the absolute error for the angle are 94.44°, 5.72° 1.9°, and 0.71° at 4 Hz, 266 Hz, 644 Hz, and 1268 Hz, respectively.

For #3 disc, the peak values of the amplitude of identified rotor unbalance are 1722.04%, 262.49%, 39.32%, 9.24%, and 11.76% at frequencies of 8 Hz, 268 Hz, 644 Hz, 814 Hz, and 1264 Hz, respectively. The peak values of the absolute error for the angle are 120.31°, 20.6°, 8.75°, 3.49°, and 11.3° at 16 Hz, 270 Hz, 644 Hz, 814 Hz, and 1268 Hz, respectively.

For #4 disc, the peak values of the amplitude of identified rotor unbalance are 853.26%, 4.43%, 13.87%, and 3.3% at frequency 6 Hz, 268 Hz, 810 Hz, and 1266 Hz, respectively. The peak values of the absolute error for the angle are 165.1°, 10.04°, 0.79°, 4.34°, and 1.5° at 10 Hz, 270 Hz, 644 Hz, 810 Hz, and 1264 Hz, respectively.

(4) Sensor resolution of 1 um

As the sensor resolution was reduced to 1 um, the starting frequency of the identification was 856 Hz (SDA does not work at a low frequency). According to Figure 24, for #1 disc, the peak value of the amplitude of identified rotor unbalance is 0.63% at a frequency of 1266 Hz. The peak value of the absolute error for the angle is 0.45° at 1262 Hz. For #2 disc, the peak value of the amplitude of identified rotor unbalance is 1.58% at a frequency of 1268 Hz. The peak value of the absolute error for the angle is 0.75° at 1268 Hz. For #3 disc, the peak value of the amplitude of identified rotor unbalance is 11.73% at a frequency of 1264 Hz. The peak value of the absolute error for the angle is 11.56° at 1268 Hz. For #4 disc, the peak value of the amplitude of identified rotor unbalance is 3.47% at a frequency of 1268 Hz. The peak value of the absolute error for the angle is 1.49° at 1264 Hz.

(5) According to the above results, the peak values that were outside the assumed allowable range—the amplitudes bigger than 20% and the angles bigger than 10°—are all counted in Tables 7–10, with the sensor resolutions set at 0.1 nm, 1 nm, 0.1 um, and 1 um, respectively. From Tables 7–10, the frequencies at which these peak values ap-

pear are at or around the critical frequencies listed in Table 11 and the low frequencies such as 1 Hz, 4 Hz, and so on. This indicates that the rotor unbalance identification error is big when the rotor works at a low speed or near the critical speeds when using SDA.

Table 7. Statistical results of peak values outside the assumed allowable range when the resolution is 0.1 nm.

Disc	Unbalance	Value	Value	Value	Value
#1	Amplitude	(10.84%, 1 Hz)	-	-	-
	Angle	-	-	-	-
#2	Amplitude	-	-	(42.54%, 645 Hz)	-
	Angle	-	-	-	-
#3	Amplitude	(26.02%, 1 Hz)	(257.24%, 269 Hz)	-	(20.64%, 1265 Hz)
	Angle	(19.49°, 1 Hz)	-	(11.72°, 645 Hz)	-
#4	Amplitude	-	-	-	-
	Angle	-	(16.259°, 269 Hz)	-	-

Table 8. Statistical results of peak values outside the assumed allowable range when the resolution is 1 nm.

Disc	Unbalance	Value	Value	Value	Value
#1	Amplitude	(83.36%, 1 Hz)	-	-	-
	Angle	-	-	-	-
#2	Amplitude	(95.6%, 1 Hz)	(42.54%, 269 Hz)	-	-
	Angle	(32.5°, 1 Hz)	-	-	-
#3	Amplitude	(242.24%, 1 Hz)	(257.24%, 269 Hz)	(11.64%, 645 Hz)	(20.64%, 1265 Hz)
	Angle	(108.42°, 1 Hz)	(57.41°, 271 Hz)	(11.72°, 645 Hz)	-
#4	Amplitude	-	-	-	-
	Angle	(165.08°, 1 Hz)	(16.259°, 269 Hz)	-	-

Table 9. Statistical results of peak values outside the assumed allowable range when the resolution is 0.1 μm.

Disc	Unbalance	Value	Value	Value	Value
#1	Amplitude	(695.26%, 4 Hz)	(19.45%, 268 Hz)	-	-
	Angle	(140.04°, 4 Hz)	(10.86°, 268 Hz)	-	-
#2	Amplitude	(597.53%, 4 Hz)	(22.7%, 270 Hz)	-	-
	Angle	(94.44°, 4 Hz)	-	-	-
#3	Amplitude	(1722.04%, 8 Hz)	(262.49%, 268 Hz)	-	(11.76%, 1268 Hz)
	Angle	(120.31°, 16 Hz)	(20.6°, 270 Hz)	-	(11.3°, 1268 Hz)
#4	Amplitude	(853.26%, 6 Hz)	-	-	-
	Angle	(165.1°, 10 Hz)	(10.04°, 270 Hz)	-	-

Table 10. Statistical results of peak values outside the assumed allowable range when the resolution is 1 μm.

Disc	Unbalance	Value
#1 disc	Amplitude	-
	Angle	-
#2 disc	Amplitude	-
	Angle	-
#3 disc	Amplitude	(11.73%, 1264 Hz)
	Angle	(11.56°, 1268 Hz)
#4 disc	Amplitude	-
	Angle	-

Table 11. First three critical frequencies of g1.4 from 1 Hz to 2000 Hz.

First Order	Second Order	Third Order
269 Hz	645 Hz	1267 Hz

Moreover, similar results can also be obtained in simulations of g4.4, h1.4, and h4.4.

3.4.2. Discussion

In the fourth kind of numerical simulation, the proposed adjustment point is applied and four kinds of typical sensor resolutions are considered for the validation of SDA. At or around the critical frequencies which are obtained by CRDAM and low frequencies, the identification error for rotor unbalance is bigger than at other frequencies. The resolution of sensors is applied by limiting the number of digits after the decimal point in the unbalance responses. At a low frequency, the unbalance responses are very small. The rounding digits have a considerable influence on small values and causes big input errors for unbalance responses. At or near the critical frequency, the unbalance responses vary greatly with frequencies. It is indicated that the rounding digits may lead to big differences among the measured errors of unbalance responses. The repeatability precision of the input responses is poor. Hence, big identification error occurs at low frequencies or at critical frequencies. Similarly, the peak values that are outside the assumed allowable range are at or around the critical frequencies and low frequencies. Far from the critical frequencies, the identification errors are small. The rotating machines' operational frequency (speed) is designed to be far from the critical frequencies to avoid resonance. This indicates that SDA can be applied to rotors not working under very low rotating speeds.

The statistical results for peak values of the identification error for #1 disc of rotor g1.4 are listed in Table 12. According to Table 12, it is indicated as follows:

- (1) At a low frequency, the peak values of identification errors become bigger as sensor resolution is reduced and rotor unbalance cannot be identified when the sensor resolution is 1 μm .
- (2) At or around the first order critical frequency, the identification error, which is obtained using a sensor resolution of 0.1 nm, is little different from the identification error obtained using a sensor resolution of 1 nm. The identification error becomes much bigger when the sensor resolution is 0.1 μm and the rotor unbalance cannot be identified when the sensor resolution is close to 1 μm .
- (3) At or around the second order critical frequency, the identification error obtained when the sensor resolution is 0.1 nm is equal to the identification error obtained when the sensor resolution is 1 nm. However, when the sensor resolution is 0.1 μm , the identification error becomes a little bigger. Moreover, when the sensor resolution comes close to 1 μm , the rotor unbalance cannot be identified.
- (4) At or around the third order critical frequency, the identification error obtained when the sensor resolution is 0.1 nm is equal to the identification error obtained when the sensor resolution is 1 nm. However, when the sensor resolution comes close to 0.1 μm and 1 μm , the identification errors become a little bigger.

The above indicates that sensors with a resolution of 1 μm should be avoided and sensors with a resolution of 1 nm and 0.1 nm are recommended for practical application. Similar results can also be obtained from the identification errors for rotor unbalance for #2~#4 discs. These indicate that SDA requires high sensor resolution. The higher the sensor resolution is, the smaller the identification error. In engineering, the resolution of most vibration displacement sensors is 1 μm and sensors with resolutions of 0.1 nm and 1 nm are very expensive. Hence, the cost of SDA can be very high when there are multiple discs and bearings in a rotor.

Table 12. Statistical results of peak values of identification errors of rotor unbalance for #1 disc in g1.4.

Sensor Resolution	Low Frequency (1 Hz)	First Order (269 Hz)	Second Order (645 Hz)	Third Order (1267 Hz)
0.1 nm	(10.84%, 1 Hz) (2.12°, 1 Hz)	(2.02%, 271 Hz) (1.47°, 271 Hz)	(0.31%, 643 Hz) (0.32°, 645 Hz)	(0.42%, 1267 Hz) (0.32°, 1267 Hz)
1 nm	(83.36%, 1 Hz) (8.77°, 1 Hz)	(1.92%, 269 Hz) (1.45°, 271 Hz)	(0.31%, 643 Hz) (0.32°, 645 Hz)	(0.42%, 1267 Hz) (0.32°, 1267 Hz)
0.1 μ m	(695.26%, 4 Hz) (140.04°, 4 Hz)	(19.45%, 268 Hz) (10.86°, 268 Hz)	(0.65%, 646 Hz) (0.55°, 646 Hz)	(0.62%, 1266 Hz) (0.45°, 1262 Hz)
1 μ m	Cannot be identified	Cannot be identified	Cannot be identified	(0.63%, 1266 Hz)
	Cannot be identified	Cannot be identified	Cannot be identified	(0.45°, 1262 Hz)

4. Conclusions

In this paper, two kinds of algorithms, SDA and TODA, are proposed to identify rotor unbalances in multi-disc and multi-span rotors from unbalance responses. Rotors are modeled based on the continuous rotor dynamic analysis method. By using the unbalance responses as inputs and considering the unbalance responses at the bearings and the eccentric discs as unknown variables, an inverse problem model is developed based on the matrix method to eliminate the coupling between bearing coefficients and rotor unbalances. Four kinds of numerical simulations considering sensor resolutions and measurement errors were conducted to study the algorithms. Compared with existing methods, the proposed algorithms have the flexibility to incorporate any number of bearings and discs. Moreover, test runs and external exciters are not required. The conclusions are summarized as follows.

- (1) The proposed algorithms provide a technique with which to monitor all the rotor unbalances on-line under operational conditions. For SDA, the unbalance responses in only one direction are needed. For a rotor with m discs and n bearings, the number of required unbalance responses is $m + n + 1$. While for TODA, the unbalance responses in both the x and y directions are required. The necessary measuring position of the two methods should be at the disc whose unbalance is to be monitored. For monitoring the unbalance of all discs, there should be a sensor mounted at each disc, while the other measuring positions can be at or around the bearings or discs. Moreover, numerical simulations indicate that there should be one measuring point called the adjustment point to achieve a high identification accuracy. The proposed adjustment point should be near the disc whose unbalance is to be monitored. In order to identify all the discs' unbalances accurately and simultaneously, there should be $m + n + n$ measuring points, among which n adjustment points near each disc are necessary.
- (2) The identification accuracy of the proposed algorithms requires a high performance of the unbalance response measurement system. Numerical simulations indicate that if the measuring errors of all the required unbalance responses are zero, the identification error will be zero, too. When the measuring errors are the same, the identification error will be equal to the measuring errors. It is indicated that the consistency of each channel's measurement errors plays a critical role in identifying rotor unbalance when using the proposed algorithms. In addition, SDA has a better identification accuracy than TODA when considering sensor resolution from the perspective of engineering applications. The identification error of SDA is only high at a very low frequency and the critical frequencies when sensor resolutions are considered. Hence, SDA is suitable for medium-speed and high-speed rotors. Moreover, identification accuracy is strongly related to sensor resolution. Sensors with resolutions of 1 μ m should be avoided and sensors with 1 nm and 0.1 nm resolutions are recommended.

For future research, there are various possible directions. Experiments should be conducted to validate the proposed methods. The limitation of the proposed algorithms is that they are not suitable for low-speed rotors and a high accuracy of measurement of unbalance responses is strongly demanded. Therefore, sensors and instruments with high accuracy and good resolutions for measuring unbalance responses should be developed. Moreover, further investigations could focus on decreasing the high requirements on measurement accuracy. Sensors with a resolution of 1 μm can be used for the identification. The Timoshenko model, in which gyroscopic moments are considered, could be taken into consideration based on CRDAM when modelling a continuous shaft. The research method of this paper can be regarded as a tool for future study.

Author Contributions: Conceptualization, A.W.; methodology, A.W.; software, A.W., Y.B. and Y.F.; formal analysis, A.W.; investigation, Y.F., X.C. and J.Y.; writing—original draft preparation, A.W. and Y.B.; writing—review and editing, A.W. and Y.B.; supervision, G.M.; funding acquisition, G.M. All authors have read and agreed to the published version of the manuscript.

Funding: This research was funded by the Fundamental Research Funds for the Central Universities, grant number 8000150A084, and the Yue Qi Young Scholar Project, China University of Mining & Technology, Beijing.

Institutional Review Board Statement: Not applicable.

Informed Consent Statement: Not applicable.

Data Availability Statement: The study did not report any data.

Conflicts of Interest: The authors declare no conflict of interest.

Nomenclature

q	Dimensionless value of position z due on the z -axis
$U(q)$	Dimensionless unbalance response in the frequency domain due on the y -axis
$V(q)$	Dimensionless unbalance response in the frequency domain due on the x -axis
#	For instance, #1 disc means the first disc
m_{ju}	Eccentric masses of # j disc
e_j	Eccentric distance of # j disc
α_j	Eccentric angle of # j disc
m_{jd}	Masses of # j disc
ω	Rotation frequency rotors
L	Length of rotor shaft
E	Elastic modulus of rotor shaft
I	Diametric shaft cross-sectional geometric moment of inertia
$k_{jj\cdot xx}$	# jj bearing's main stiffness coefficient in the x direction
$k_{jj\cdot xy}$	# jj bearing's cross-coupled stiffness coefficient in the x direction
$k_{jj\cdot yx}$	# jj bearing's cross-coupled stiffness coefficient in the y direction
$k_{jj\cdot yy}$	# jj bearing's main stiffness coefficient in the y direction
$c_{jj\cdot xx}$	# jj bearing's main damping coefficient in the x direction
$c_{jj\cdot xy}$	# jj bearing's cross-coupled damping coefficient in the x direction
$c_{jj\cdot yx}$	# jj bearing's cross-coupled damping coefficient in the y direction
$c_{jj\cdot yy}$	# jj bearing's main damping coefficient in the y direction
$k_{s\cdot xx}$	Bearing's main complex coefficient in the x direction
$k_{s\cdot xy}$	Bearing's cross-coupled complex coefficient in the x direction
$k_{s\cdot yx}$	Bearing's cross-coupled complex coefficient in the y direction
$k_{s\cdot yy}$	Bearing's main complex coefficient in the y direction
z_{jd}	z coordinate position of # j disc
z_{jyb}	z coordinate position of # jj bearing
q_{jd}	Dimensionless value of z_{jd}
q_{jyb}	Dimensionless value of z_{jyb}

$G_u(q, q_i)$	Green's functions in the y direction
$G_v(q, q_i)$	Green's functions in the x direction
$G_u(q, q_{jd})$	Green's coefficients for # j disc in the y direction
$G_u(q, q_{jyb})$	Green's coefficients for # j bearing in the y direction
$G_v(q, q_{jd})$	Green's coefficients for # j disc in the x direction
$G_v(q, q_{jyb})$	Green's coefficients for # j bearing in the x direction
U_{jd}	# j disc's dimensionless unbalance response in frequency domain in the y direction
V_{jd}	# j disc's dimensionless unbalance response in frequency domain in the x direction
U_{jyb}	# j bearing's dimensionless unbalance response in frequency domain in the y direction
V_{jyb}	# j bearing's dimensionless unbalance response in frequency domain in the x direction
m	Number of discs
n	Number of bearings

Appendix A

(1) Simulation results for g1.1 and h1.1

In this simulation, #60 and #30 are used as the required measuring points for g1.1 and h1.1, respectively, and the other measuring points are at the locations of the two bearings and the disc.

Table A1. The maximum identification errors of the disc calculated by SDA and TODA.

Methods	Rotor Unbalance	g1.1	h1.1
SDA	Amplitude	6.77977×10^{-9}	1.23934×10^{-8}
	Angle	1.6455×10^{-9}	7.73824×10^{-9}
TODA	Amplitude	4.21247×10^{-5}	2.79355×10^{-8}
	Angle	3.32871×10^{-6}	2.49249×10^{-8}

(2) Simulation results for rotor h4.4

In this simulation, #10 is used as one of the required measuring points and the other measuring points are at the locations of the two bearings and the four discs.

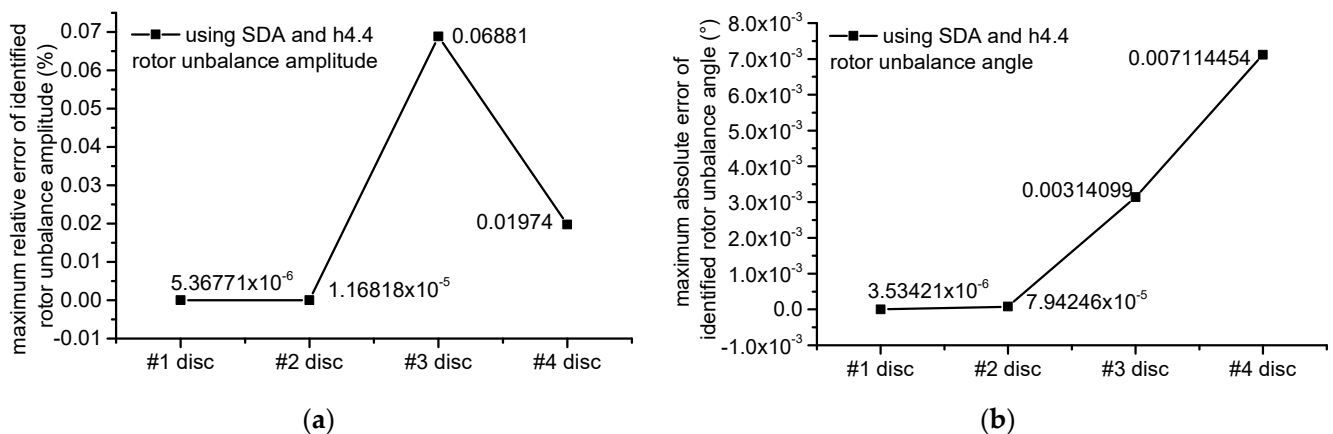


Figure A1. The maximum identification error for each rotor unbalance in h4.4 based on SDA using #10 point as one of the required measuring points: (a) relative error for rotor unbalance amplitude; (b) absolute error for rotor unbalance angle.

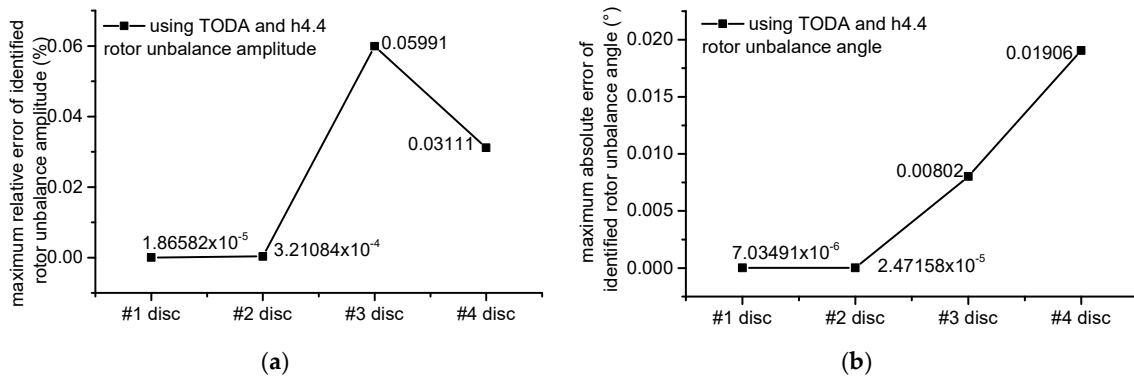


Figure A2. The maximum identification error for each rotor unbalance in h4.4 based on TODA using #10 point as one of the required measuring points: (a) relative error for the rotor unbalance amplitude; (b) absolute error for the rotor unbalance angle.

(3) Simulation results for rotor g1.4

In this simulation, #20 is used as one of the required measuring points and the other measuring points are #15, #90, #21, #41, #61, and #81, which are the locations of the two bearings and the four discs.

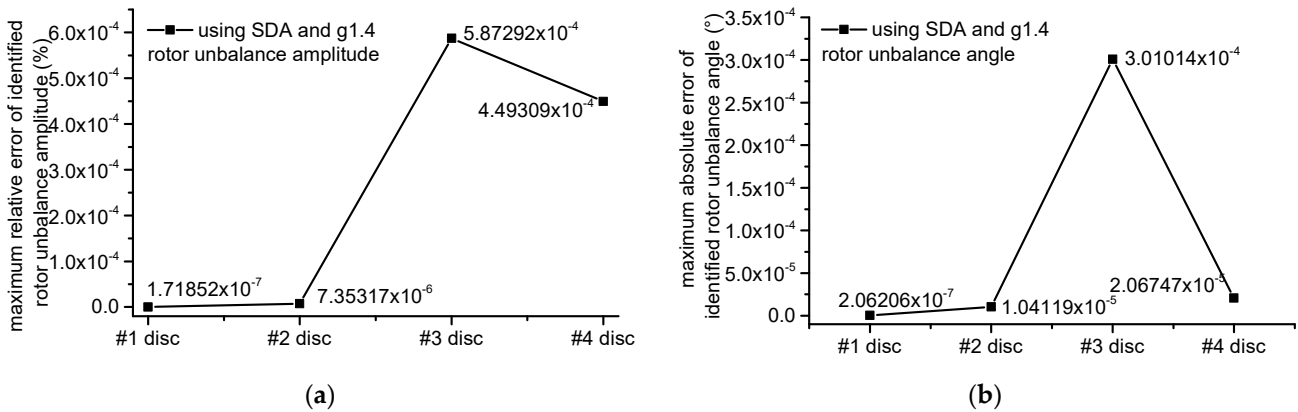


Figure A3. The maximum identification error for each rotor unbalance in g1.4 based on SDA using #20 point as one of the required measuring points: (a) relative error for the rotor unbalance amplitude; (b) absolute error for the rotor unbalance angle.

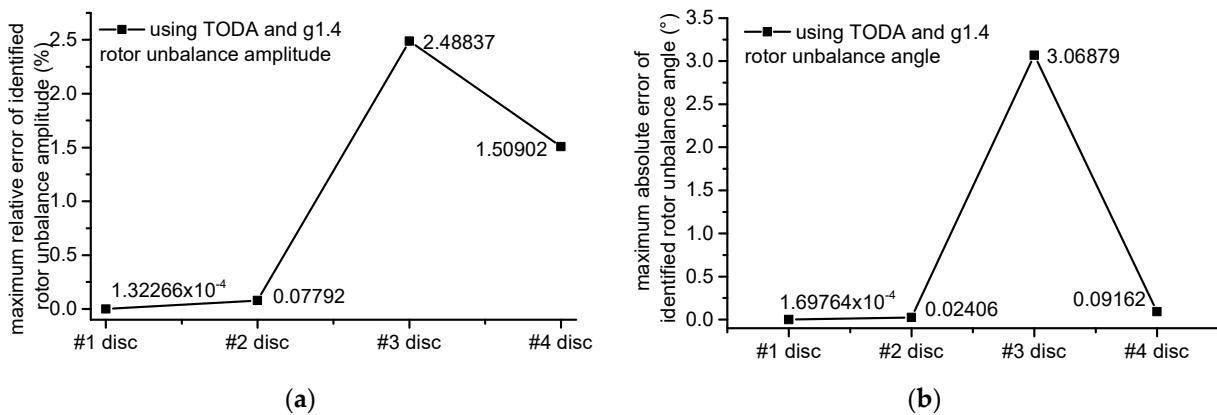


Figure A4. The maximum identification error for each rotor unbalance in g1.4 based on TODA using #20 point as one of the required measuring points: (a) relative error for rotor unbalance amplitude; (b) absolute error for rotor unbalance angle.

Appendix B

(1) Simulation results for g1.1 and h1.1

In this simulation, #60 and #30 are used as one of the required measuring points for g1.1 and h1.1, respectively, and the other measuring points are at the locations of the two bearings and the disc.

Table A2. The maximum identification error for the disc calculated by SDA and TODA.

Methods	Rotor Unbalance	G1.1	H1.1
SDA	Amplitude	5.00000007	5.000000013
	Angle	5	5.000000008
TODA	Amplitude	5.000000108	5.000000022
	Angle	5.000003329	5.000000025

(2) Simulation results for rotor g1.4

In this simulation, #20 is used as one of the required measuring points and the other measuring points are #15, #90, #21, #41, #61, and #81, where the two bearings and the four discs are.

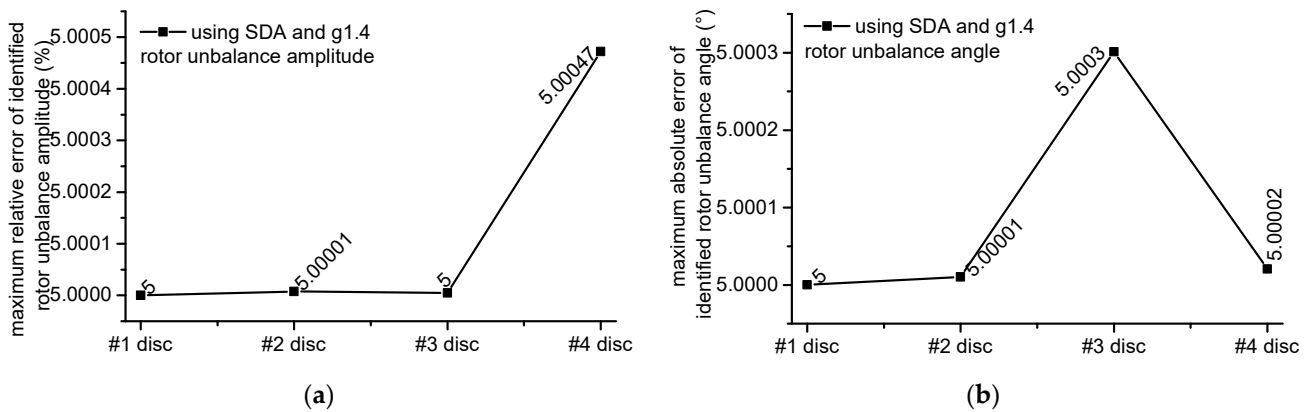


Figure A5. The maximum identification error for each rotor unbalance in g1.4 based on SDA using #20 point as one of the required measuring points: (a) relative error for the rotor unbalance amplitude; (b) absolute error for the rotor unbalance angle.

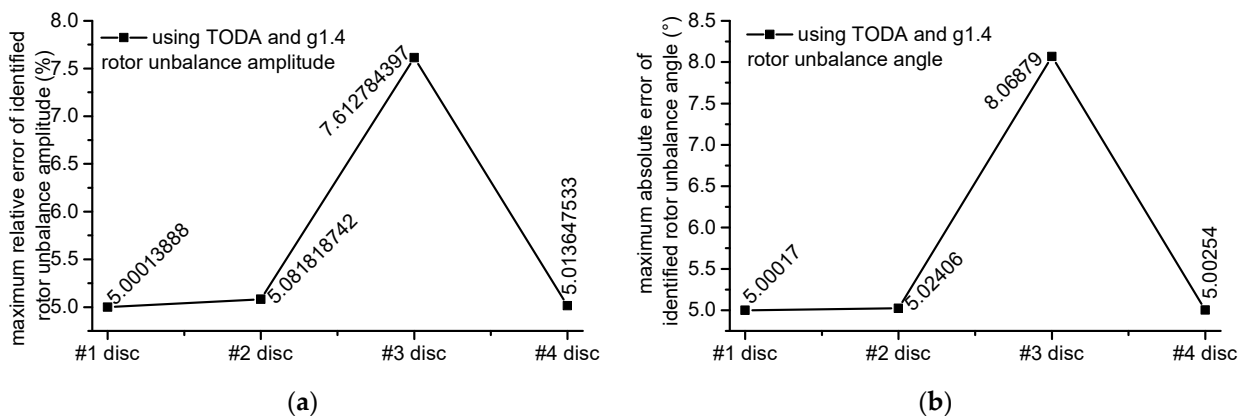


Figure A6. The maximum identification error for each rotor unbalance in g1.4 based on TODA using #20 point as one of the required measuring points: (a) relative error for the rotor unbalance amplitude; (b) absolute error for the rotor unbalance angle.

(3) Simulation results for rotor h4.4

In this simulation, #10 is used as one of the required measuring points and the other measuring points are at the locations of the two bearings and the four discs.

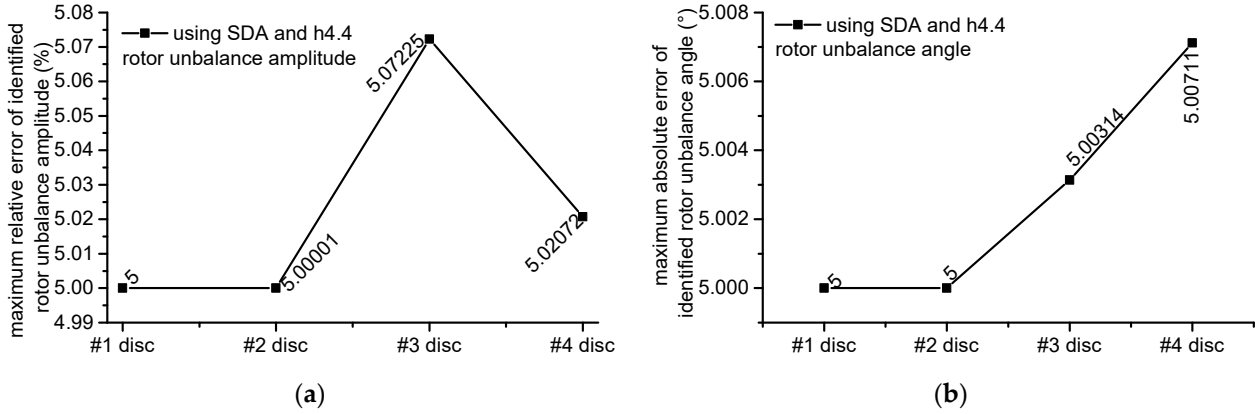


Figure A7. The maximum identification error for each rotor unbalance in h4.4 based on SDA using #10 point as one of the required measuring points: (a) relative error for the rotor unbalance amplitude; (b) absolute error for the rotor unbalance angle.

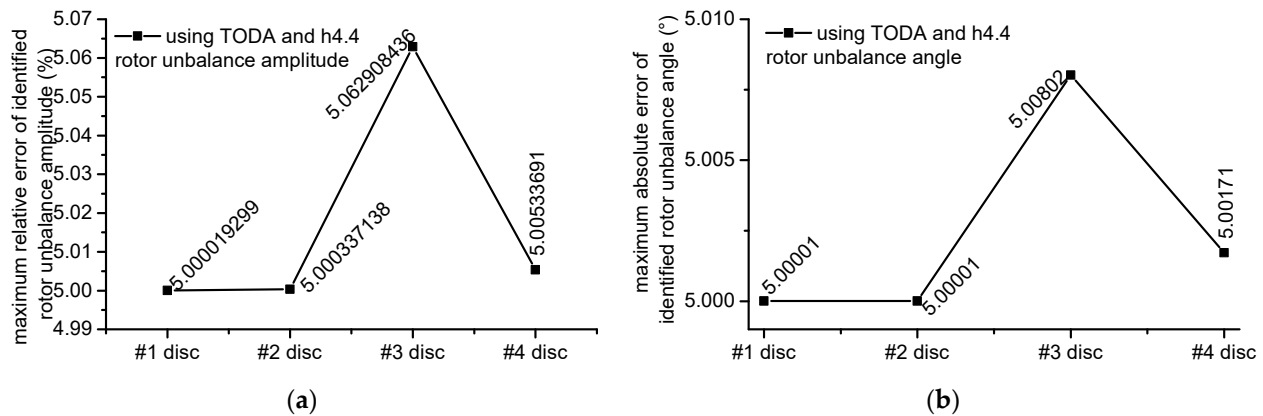


Figure A8. The maximum identification error for each rotor unbalance in h4.4 based on TODA using #10 point as one of the required measuring points: (a) relative error for the rotor unbalance amplitude; (b) absolute error for the rotor unbalance angle.

Appendix C

(1) Simulation results for g4.4

In this simulation, #20, #40, #60, and #80 points are used, respectively, and the other $m + n$ measuring points are at the discs and bearings.

$$SDA_M1_{g44} = \begin{bmatrix} 7.74 & 7263.22 & 4675809.49 & 38337218.12 \\ 290.65 & 4.75 & 15819.92 & 131153.82 \\ 47436.53 & 2396.85 & 270.45 & 2287.39 \\ 2659853.86 & 134047.34 & 11889.74 & 4.97 \end{bmatrix} \quad (A1)$$

$$SDA_M2_{g44} = \begin{bmatrix} 0.70 & 176.85 & 179.33 & 178.63 \\ 94.64 & 8.20 & 177.39 & 179.98 \\ 179.58 & 170.81 & 19.58 & 104.65 \\ 171.64 & 177.59 & 138.72 & 1.63 \end{bmatrix} \quad (A2)$$

$$TODA_M1_{g44} = \begin{bmatrix} 2.72 \times 10^3 & 2.20 \times 10^5 & 6.15 \times 10^8 & 5.97 \times 10^9 \\ 4.66 \times 10^4 & 5.71 \times 10^3 & 7.17 \times 10^6 & 6.97 \times 10^7 \\ 7.48 \times 10^6 & 3.64 \times 10^4 & 4.97 \times 10^4 & 1.78 \times 10^5 \\ 3.49 \times 10^9 & 1.60 \times 10^7 & 6.20 \times 10^6 & 1.27 \times 10^4 \end{bmatrix} \quad (A3)$$

$$TODA_M2_{g44} = \begin{bmatrix} 172.85 & 177.23 & 173.68 & 175.19 \\ 179.57 & 115.55 & 179.88 & 179.76 \\ 179.98 & 179.66 & 178.09 & 179.98 \\ 179.92 & 179.92 & 179.91 & 177.42 \end{bmatrix} \quad (A4)$$

where SDA_M1_{g44} and SDA_M2_{g44} are the matrix of the maximum identification error for rotor unbalance amplitude and the angle of #1 to #4 discs under different adjustment point conditions using SDA; $TODA_M1_{g44}$ and $TODA_M2_{g44}$ are the matrix of the maximum identification error for rotor unbalance amplitude and the angle of #1 to #4 discs under different adjustment point conditions using TODA.

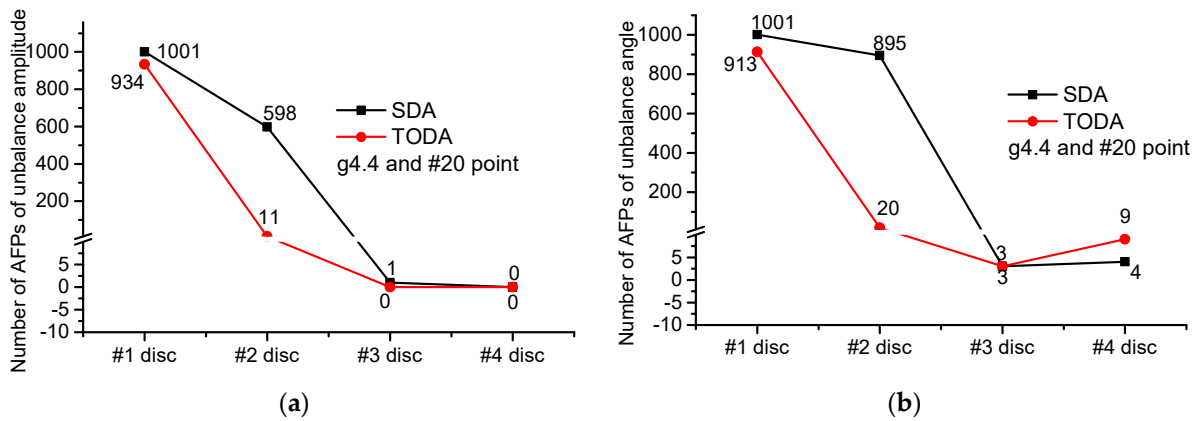


Figure A9. Statistical results of the number of AFPs of rotor unbalance of each disc in the simulation of g4.4 using #20 point as one of the required measuring points and a 0.1 nm resolution: (a) results of unbalance amplitude; (b) results of unbalance angle.

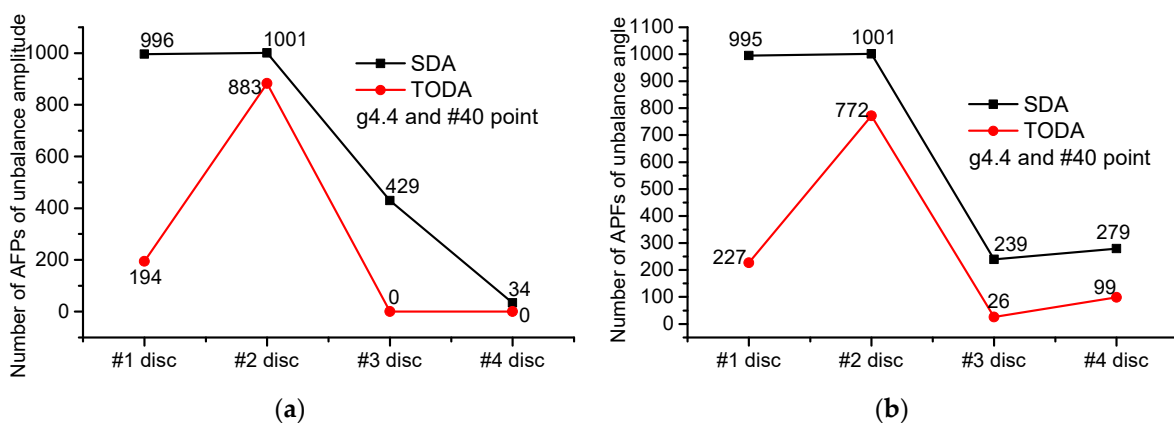


Figure A10. Statistical results of the number of AFPs of rotor unbalance of each disc in the simulation of g4.4 using #40 point as one of the required measuring points and a 0.1 nm resolution: (a) results of unbalance amplitude; (b) results of unbalance angle.

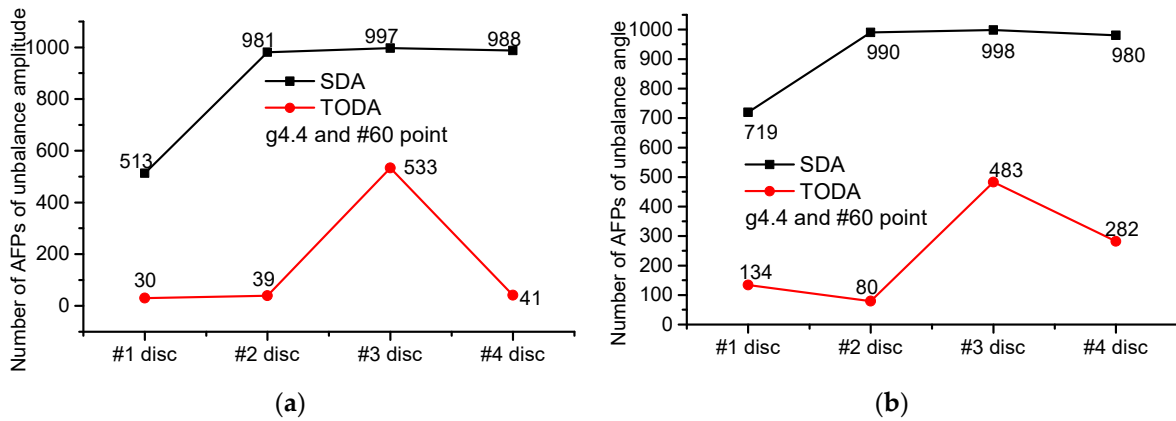


Figure A11. Statistical results of the number of AFPs of rotor unbalance of each disc in the simulation of g4.4 using #60 point as one of the required measuring points and a 0.1 nm resolution: (a) results of unbalance amplitude; (b) results of unbalance angle.

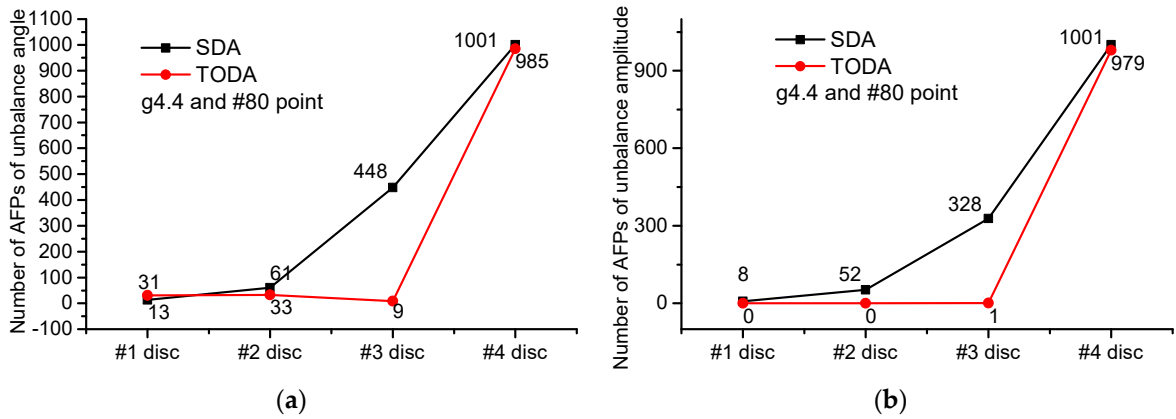


Figure A12. Statistical results of the number of AFPs of rotor unbalance of each disc in the simulation of g4.4 using #80 point as one of the required measuring points and a 0.1 nm resolution: (a) results of unbalance amplitude; (b) results of unbalance angle.

(2) Simulation results for h1.4

In this simulation, #10, #20, #30, and #40 points are used, respectively, and the other $m + n$ measuring points are at the discs and bearings.

$$SDA_M1_{h14} = \begin{bmatrix} 62.06 & 377.46 & 15340.98 & 8311.13 \\ 495.48 & 9.29 & 5473.69 & 3128.49 \\ 1050.54 & 302.84 & 146.67 & 515.27 \\ 1741.08 & 422.80 & 650.49 & 42.56 \end{bmatrix} \quad (A5)$$

$$SDA_M2_{h14} = \begin{bmatrix} 21.67 & 176.86 & 178.86 & 179.80 \\ 119.47 & 7.69 & 172.06 & 179.22 \\ 142.30 & 139.97 & 136.16 & 163.97 \\ 140.05 & 83.30 & 170.82 & 12.68 \end{bmatrix} \quad (A6)$$

$$TODA_M1_{h14} = \begin{bmatrix} 678.59 & 11343.28 & 126989.97 & 68381.74 \\ 9068.03 & 611.79 & 96905.97 & 20941.13 \\ 41233.01 & 8545.67 & 4524.67 & 5890.04 \\ 91145.20 & 24188.79 & 18490.77 & 294.55 \end{bmatrix} \quad (A7)$$

$$TODA_M2_{h14} = \begin{bmatrix} 151.57 & 171.11 & 179.62 & 179.20 \\ 175.38 & 134.00 & 179.86 & 177.95 \\ 176.74 & 165.76 & 173.57 & 179.56 \\ 179.20 & 179.39 & 179.86 & 107.60 \end{bmatrix} \quad (A8)$$

where SDA_M1_{h14} and SDA_M2_{h14} are the matrix of the maximum identification error for rotor unbalance amplitude and the angle of #1 to #4 discs under different adjustment point conditions using SDA; $TODA_M1_{h14}$ and $TODA_M2_{h14}$ are the matrix of the maximum identification error for rotor unbalance amplitude and the angle of #1 to #4 discs under different adjustment point conditions using TODA.

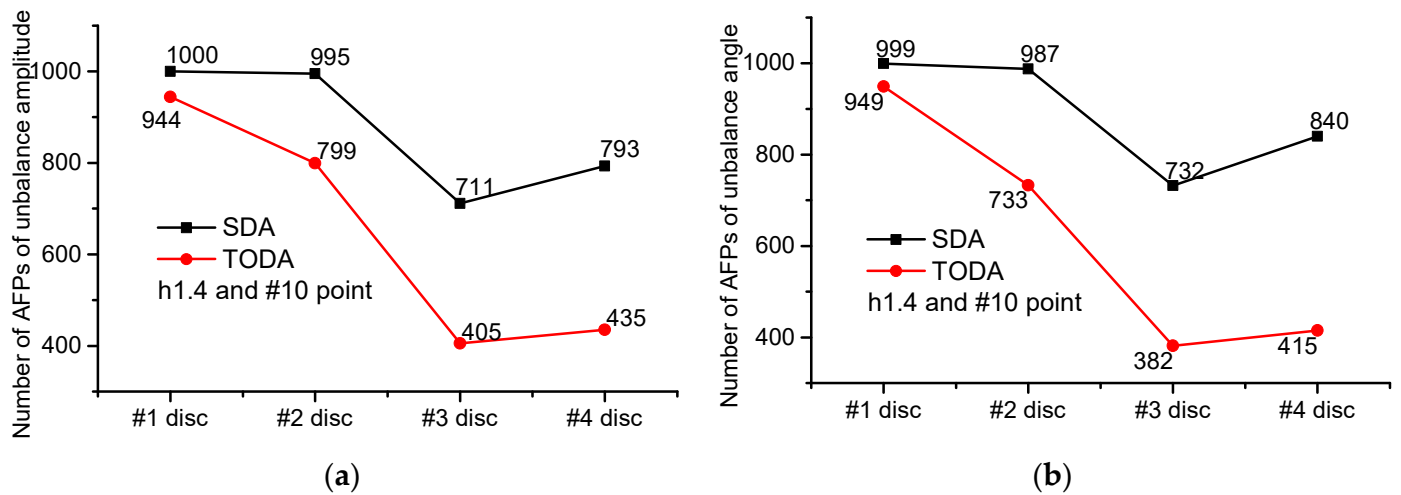


Figure A13. Statistical results of the number of AFPs of rotor unbalance of each disc in the simulation of h1.4 using #10 point as one of the required measuring points and a 0.1 nm resolution: (a) results of unbalance amplitude; (b) results of unbalance angle.

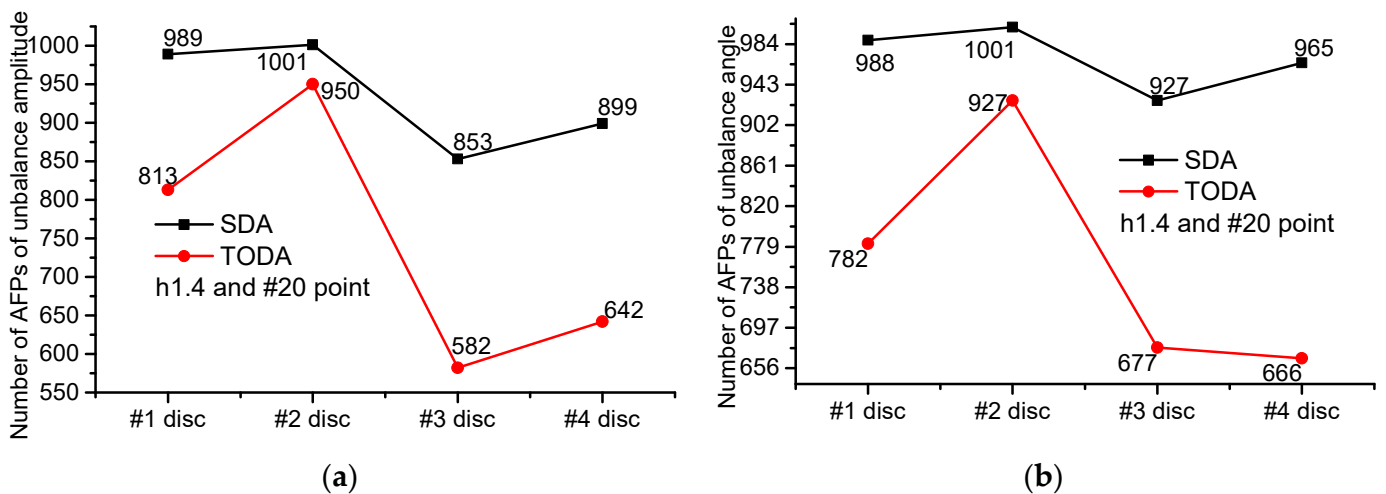


Figure A14. Statistical results of the number of AFPs of rotor unbalance of each disc in the simulation of h1.4 using #20 point as one of the required measuring points and a 0.1 nm resolution: (a) results of unbalance amplitude; (b) results of unbalance angle.

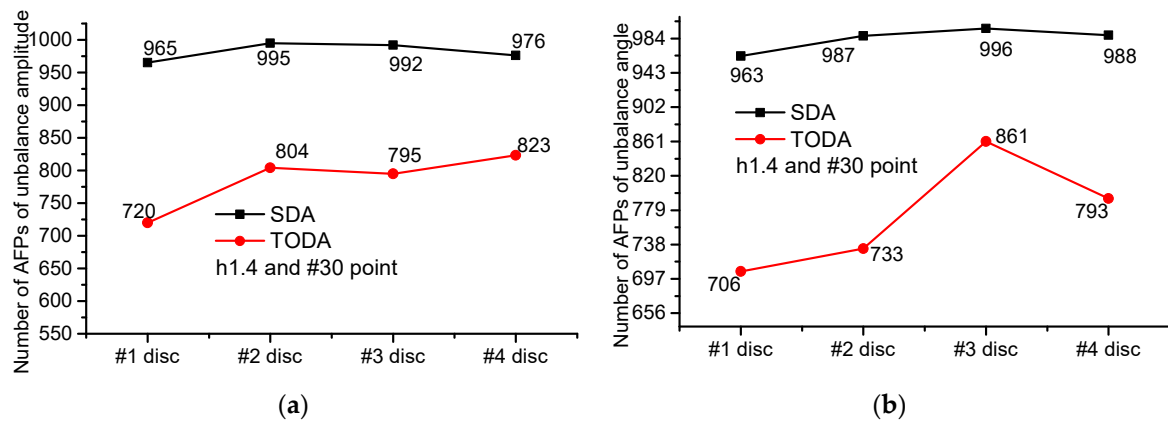


Figure A15. Statistical results of the number of AFPs of rotor unbalance of each disc in the simulation of h1.4 using #30 point as one of the required measuring points and a 0.1 nm resolution: (a) results of unbalance amplitude; (b) results of unbalance angle.

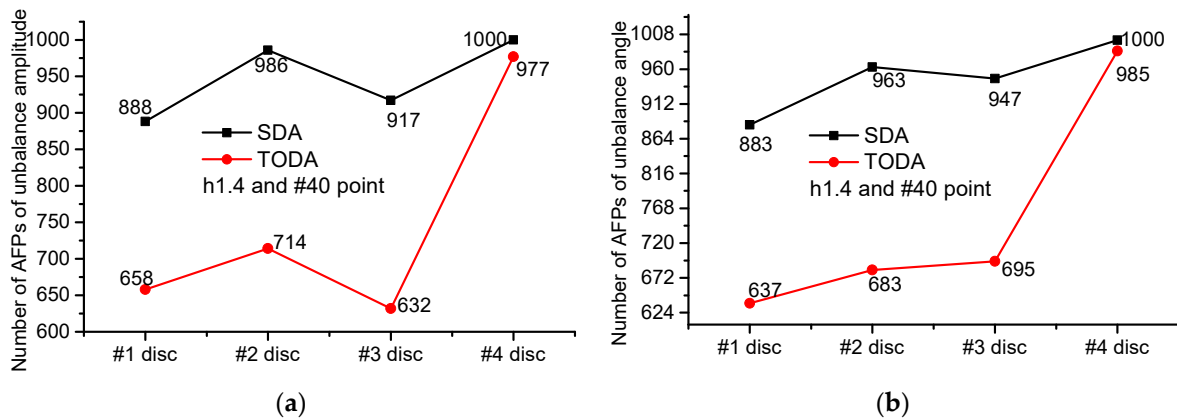


Figure A16. Statistical results of the number of AFPs of rotor unbalance of each disc in the simulation of h1.4 using #40 point as one of the required measuring points and a 0.1 nm resolution: (a) results of unbalance amplitude; (b) results of unbalance angle.

(3) Simulation results for h4.4

In this simulation, #10, #20, #30, and #40 points are used, respectively, and the other $m + n$ measuring points are at the discs and bearings.

$$SDA_M1_{h44} = \begin{bmatrix} 0.10 & 40.21 & 648.96 & 330916.69 \\ 32.56 & 1.24 & 5473.69 & 5238.11 \\ 438.92 & 44.95 & 4.46 & 61.05 \\ 132071.11 & 3609.63 & 402.43 & 1.49 \end{bmatrix} \quad (A9)$$

$$SDA_M2_{h44} = \begin{bmatrix} 0.03 & 45.47 & 179.93 & 178.81 \\ 25.58 & 0.22 & 114.52 & 179.55 \\ 179.59 & 12.10 & 6.72 & 47.90 \\ 179.90 & 178.59 & 71.69 & 0.15 \end{bmatrix} \quad (A10)$$

$$TODA_M1_{h44} = \begin{bmatrix} 0.73 & 764.47 & 28245.31 & 862557.51 \\ 3091.55 & 10.72 & 469.71 & 34447.58 \\ 43906.69 & 387.83 & 16.43 & 624.62 \\ 9631294.06 & 30595.13 & 267.13 & 6.50 \end{bmatrix} \quad (A11)$$

$$TODA_M2_{h44} = \begin{bmatrix} 0.56 & 179.40 & 179.89 & 179.22 \\ 172.28 & 6.54 & 179.54 & 179.97 \\ 178.12 & 143.85 & 5.10 & 166.32 \\ 179.77 & 174.86 & 167.72 & 5.17 \end{bmatrix} \quad (A12)$$

where SDA_M1_{h44} and SDA_M2_{h44} are the matrix of the maximum identification error for rotor unbalance amplitude and the angle of #1 to #4 discs under different adjustment point conditions using SDA; $TODA_M1_{h44}$ and $TODA_M2_{h44}$ are the matrix of the maximum identification error for rotor unbalance amplitude and the angle of #1 to #4 discs under different adjustment point conditions using TODA.

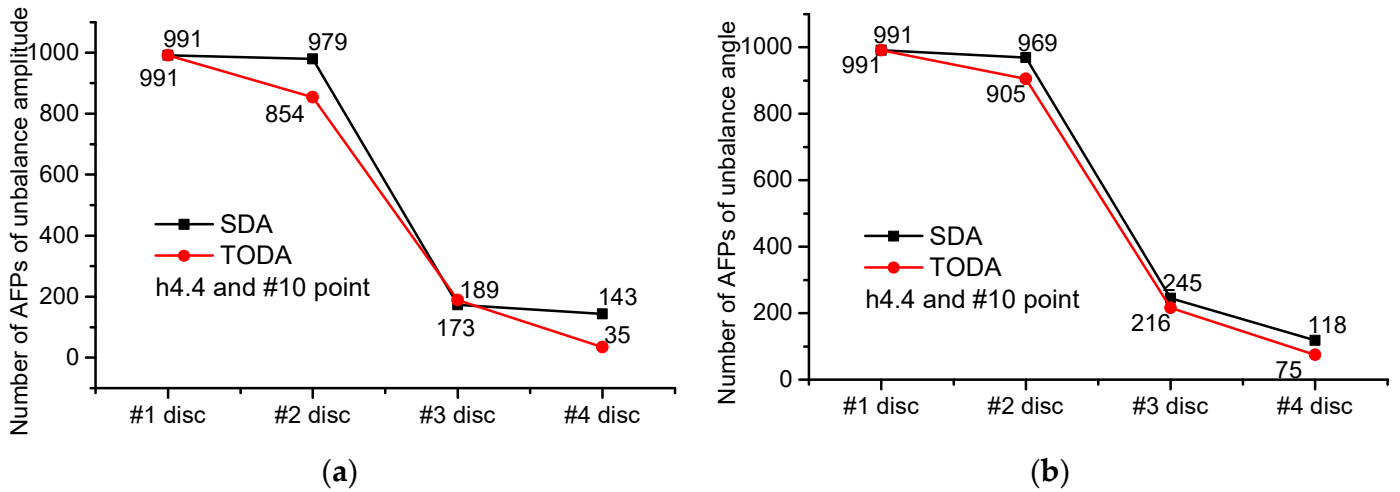


Figure A17. Statistical results of the number of AFPs of rotor unbalance of each disc in the simulation of h4.4 using #10 point as one of the required measuring points and a 0.1 nm resolution: (a) results of unbalance amplitude; (b) results of unbalance angle.

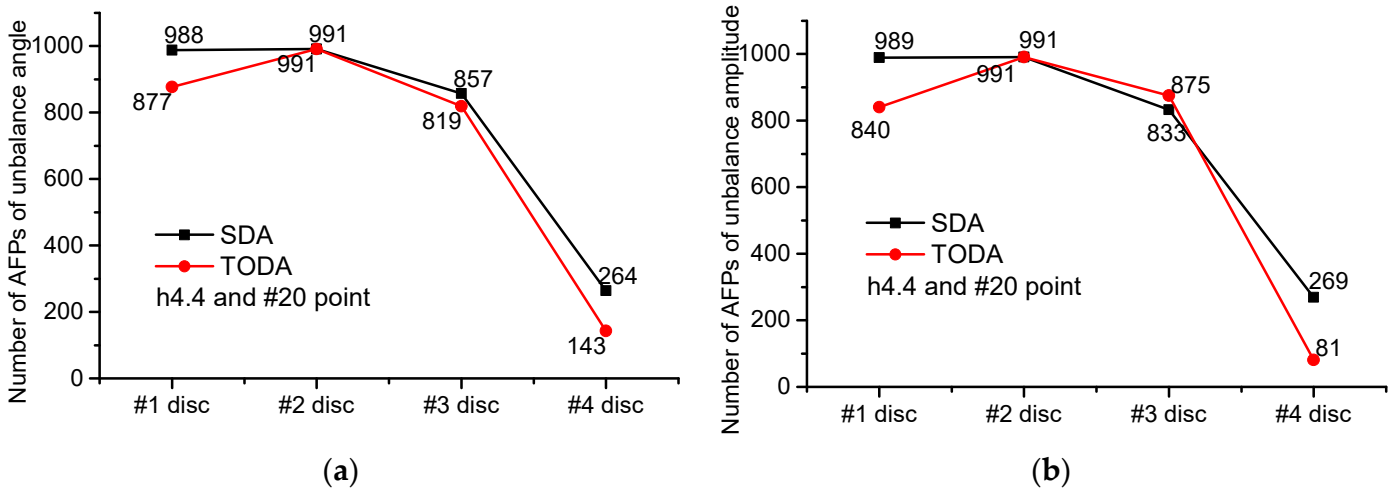


Figure A18. Statistical results of the number of AFPs of rotor unbalance of each disc in the simulation of h4.4 using #20 point as one of the required measuring points and a 0.1 nm resolution: (a) results of unbalance amplitude; (b) results of unbalance angle.

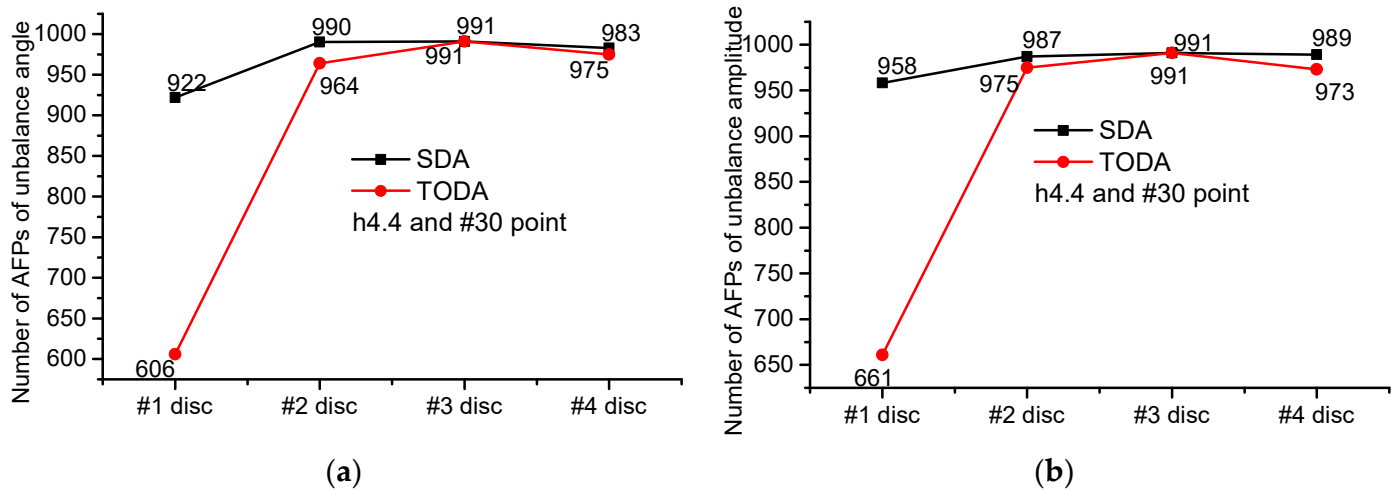


Figure A19. Statistical results of the number of AFPs of rotor unbalance of each disc in the simulation of h4.4 using #40 point as one of the required measuring points and a 0.1 nm resolution: (a) results of unbalance amplitude; (b) results of unbalance angle.

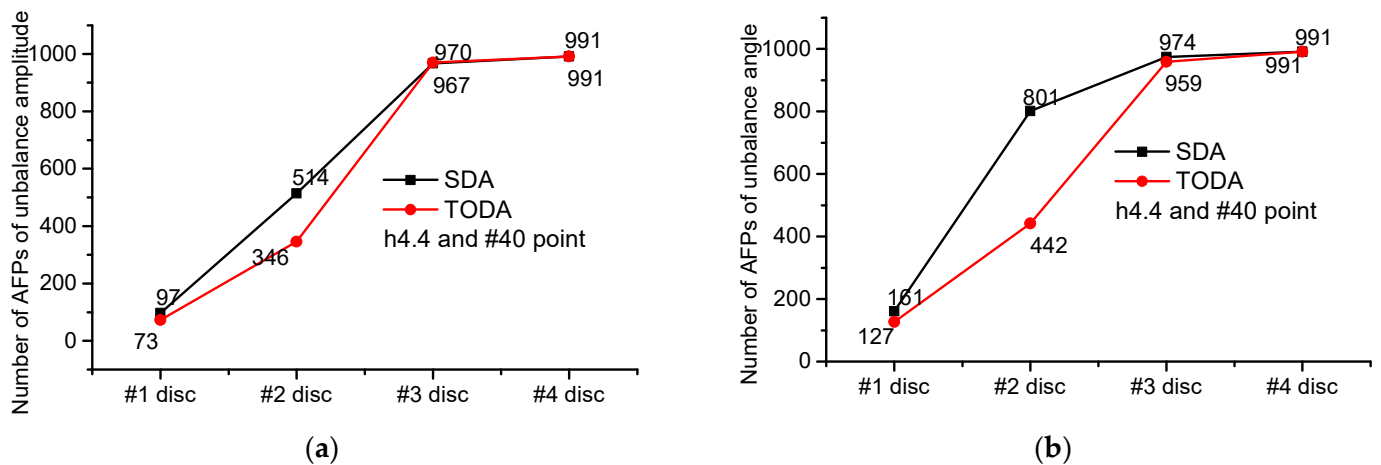


Figure A20. Statistical results of the number of AFPs of rotor unbalance of each disc in the simulation of h4.4 using #40 point as one of the required measuring points and a 0.1 nm resolution: (a) results of unbalance amplitude; (b) results of unbalance angle.

References

1. Bishop, R.E.D. The vibration of rotating shafts. *J. Mech. Eng. Sci.* **1959**, *1*, 50–65. [[CrossRef](#)]
2. Gladwell, G.M.L.; Bishop, R.E.D. The vibration of rotating shafts supported in flexible bearings. *J. Mech. Eng. Sci.* **1959**, *1*, 195–206. [[CrossRef](#)]
3. Goodman, T.P. A least-squares method for computing balance corrections. *Trans. ASME J. Eng. Ind.* **1964**, *864*, 273–279. [[CrossRef](#)]
4. Bishop, R.E.D.; Gladwell, G.M.L. The vibration and balancing of an unbalanced flexible rotor. *J. Mech. Eng. Sci.* **1959**, *1*, 66–67. [[CrossRef](#)]
5. Bishop, R.E.D.; Parkinson, A.G. On the isolation of modes in the balancing of flexible shafts. *Proc. Inst. Mech. Eng.* **1963**, *177*, 407–426.
6. Lindley, A.L.G.; Bishop, R.E.D. Some recent research of the balancing of large flexible rotors. *Proc. Inst. Mech. Eng.* **1963**, *177*, 881–897. [[CrossRef](#)]
7. Bishop, R.E.D.; Parkinson, A.G. On the use of balancing machines for flexible rotors. *ASME J. Eng. Ind.* **1972**, *94*, 561–576. [[CrossRef](#)]
8. Kellenberger, W. Balancing flexible rotors on two generally flexible bearings. *Brown Boveri Rev.* **1970**, *54*, 603–619.
9. Kellenberger, W. Should a flexible rotor be balanced in N or N + 2 planes? *Trans. ASME J. Eng. Ind.* **1972**, *94*, 548–560. [[CrossRef](#)]
10. Lund, J.W.; Tonnesen, J. Analysis and experiments in multi-plane balancing of flexible rotors. *Trans. ASME J. Eng. Ind.* **1972**, *194*, 70–77. [[CrossRef](#)]

11. Lund, J.W.; Tonnesen, J. *Experimental and Analytic Investigation of High-Speed Rotor Balancing-Phase I*; Research Report No. FR-8, Project No. FP-4; Department of Mechine Design, Technical University of Denmark: Copenhagen, Denmark, 1970.
12. Shamsah, S.M.I.; Sinha, J.K.; Mandal, P. Estimating rotor unbalance from a single run-up and using reduced sensors. *Measurement* **2019**, *136*, 11–24. [[CrossRef](#)]
13. Liu, Y.; Zhang, M.; Sun, C.; Hu, M.; Chen, D.; Liu, Z.; Tan, J. A method to minimize stage-by-stage initial unbalance in the aero engine assembly of multistage rotors. *Aerosp. Sci. Technol.* **2019**, *85*, 270–276. [[CrossRef](#)]
14. Bin, G.; Li, X.; Shen, Y.; Wang, W. Development of whole-machine high speed balance approach for turbomachinery shaft system with N + 1 supports. *Measurement* **2018**, *122*, 368–379. [[CrossRef](#)]
15. Xia, Y.; Ren, X.; Qin, W.; Yang, Y.; Lu, K.; Fu, C. Investigation on the transient response of a speed-varying rotor with sudden unbalance and its application in the unbalance identification. *J. Low Freq. Noise Vib. Act. Control* **2019**, *39*, 1065–1086. [[CrossRef](#)]
16. Bently, D.E.; Muszynska, A. Modal testing and parameter identification of rotating shaft fluid lubricated bearing system. In Proceedings of the 4th International Conference on Modal Analysis, Orlando, FL, USA, April 1986; pp. 1393–1402. Available online: https://xueshu.baidu.com/usercenter/paper/show?paperid=635ff95826102054142b1957b8cde2db&site=xueshu_se&hitarticle=1 (accessed on 16 March 2022).
17. Iida, H. Application of the Experimental Determination of Character Matrices to the Balancing of a Flexible Rotor. In Proceedings of the IFToMM 4th International Conference on Rotor Dynamics, Chicago, IL, USA, September 1994; pp. 111–115. Available online: https://xueshu.baidu.com/usercenter/paper/show?paperid=f42b876c8d2000aa6dd8baf7b534a8e8&site=xueshu_se&hitarticle=1 (accessed on 16 March 2022).
18. Lou, X.; Zheng, S.; Wang, X. Some factors of leading to nonlinear electromagnetic force in active magnetic actuator. *J. Mech. Electr. Eng.* **1999**, *2*, 40–42.
19. Liu, S.; Zheng, S. On-line unbalance identification of flexible rotor system. *J. Zhejiang Univ.* **2004**, *38*, 257–261.
20. Shrivastava, A.; Mohanty, A.R. Estimation of single plane unbalance parameters of a rotor-bearing system using Kalman filtering based force estimation technique. *J. Sound Vib.* **2018**, *418*, 184–199. [[CrossRef](#)]
21. Gillijns, S.; De Moor, B. Technical communique: Unbiased minimum-variance input and state estimation for linear discrete-time systems with direct feedthrough. *Automatica* **2007**, *43*, 934–937. [[CrossRef](#)]
22. Shrivastava, A.; Mohanty, A.R. Identification of unbalance in a rotor system using a joint input-state estimation technique. *J. Sound Vib.* **2019**, *442*, 414–427. [[CrossRef](#)]
23. Yao, J.; Liu, L.; Yang, F.; Scarpa, F.; Gao, J. Identification and optimization of unbalance parameters in rotor-bearing systems. *J. Sound Vib.* **2018**, *431*, 54–69. [[CrossRef](#)]
24. Zou, D.; Zhao, H.; Liu, G.; Ta, N.; Rao, Z. Application of augmented Kalman filter to identify unbalance load of rotor-bearing system: Theory and experiment. *J. Sound Vib.* **2019**, *463*, 114972. [[CrossRef](#)]
25. He, C.H.; Amer, T.S.; Tian, D.; Abolila, A.F.; Galal, A.A. Controlling the kinematics of a spring-pendulum system using an energy harvesting device. *J. Low Freq. Noise Vib. Act. Control* **2022**. [[CrossRef](#)]
26. He, J.H.; Amer, T.S.; Abolila, A.F.; Galal, A.A. Stability of three degrees-of-freedom auto-parametric system. *Alex. Eng. J.* **2022**, *61*, 8393–8415. [[CrossRef](#)]
27. Wang, A.; Cheng, X.; Meng, G.; Xia, Y.; Wo, L.; Wang, Z. Dynamic analysis and numerical experiments for balancing of the continuous single-disc and single-span rotor-bearing system. *Mech. Syst. Signal Process.* **2017**, *86*, 151–176. [[CrossRef](#)]
28. Tiwari, R.; Chakravarthy, V. Simultaneous estimation of the residual unbalance and bearing dynamic parameters from the experimental data in a rotor-bearing system. *Mech. Mach. Theory* **2009**, *44*, 792–812. [[CrossRef](#)]
29. Tiwari, R. Conditioning of regression matrices for simultaneous estimation of the residual unbalance and bearing dynamic parameters. *Mech. Syst. Signal Process.* **2005**, *19*, 1082–1095. [[CrossRef](#)]
30. Wang, A.; Yao, W.; He, K.; Meng, G.; Cheng, X.; Yang, J. Analytical modelling and numerical experiment for simultaneous identification of unbalance and rolling-bearing coefficients of the continuous single-disc and single-span rotor-bearing system with Rayleigh beam model. *Mech. Syst. Signal Process.* **2019**, *116*, 322–346. [[CrossRef](#)]
31. Jamadar, I.M. A Model to Estimate Synchronous Vibration Amplitude for Detection of Unbalance in Rotor-Bearing System. *Int. J. Acoust. Vib.* **2021**, *26*, 161–169. [[CrossRef](#)]
32. Ambur, R.; Rinderknecht, S. Unbalance detection in rotor systems with active bearings using self-sensing piezoelectric actuators. *Mech. Syst. Signal Process.* **2018**, *102*, 72–86. [[CrossRef](#)]
33. Sanches, F.D.; Pederiva, R. Simultaneous identification of unbalance and shaft bow in a two-disk rotor based on correlation analysis and the SEREP model order reduction method. *J. Sound Vib.* **2018**, *433*, 230–247. [[CrossRef](#)]
34. Zhang, Y.; Li, M.; Yao, H.; Gou, Y.; Wang, X. A modal-based balancing method for a high-speed rotor without trial weights. *Mech. Sci.* **2021**, *12*, 85–96. [[CrossRef](#)]
35. Tiwari, R.; Chakravarthy, V. Simultaneous identification of residual unbalances and bearing dynamic parameters from impulse responses of rotor-bearing systems. *Mech. Syst. Signal Process.* **2006**, *20*, 1590–1614. [[CrossRef](#)]
36. Tiwari, R.; Chakravarthy, V. Identification of the bearing and unbalance parameters from rundown data of rotors. In *IUTAM Symposium on Emerging Trends in Rotor Dynamics*; Springer: Dordrecht, The Netherlands, 2011; pp. 479–489.